
Collaborative non-parametric two-sample testing

Alejandro de la Concha¹ Nicolas Vayatis¹ Argyris Kalogeratos¹

Abstract

This paper addresses the multiple two-sample test problem in a graph-structured setting, which is a common scenario in fields such as Spatial Statistics and Neuroscience. Each node v in fixed graph deals with a two-sample testing problem between two node-specific probability density functions (pdfs), p_v and q_v . The goal is to identify nodes where the null hypothesis $p_v = q_v$ should be rejected, under the assumption that connected nodes would yield similar test outcomes. We propose the non-parametric *collaborative two-sample testing* (CTST) framework that efficiently leverages the graph structure and minimizes the assumptions over p_v and q_v . Our methodology integrates elements from ϕ -divergence estimation, Kernel Methods, and Multitask Learning. We use synthetic experiments and a real sensor network detecting seismic activity to demonstrate that CTST outperforms state-of-the-art non-parametric statistical tests that apply at each node independently, hence disregard the geometry of the problem.

1. Introduction

Given two probability density functions (pdfs) p and q , a *Two-sample Test* (TST) assesses if there is significant evidence that the null hypothesis, $H_{\text{null}} : p = q$, is true, versus the alternative $H_{\text{alt}} : p \neq q$. TST has been studied in detail in the Machine Learning literature leading to several methods (Sugiyama et al., 2011b; Gretton et al., 2012; Harchaoui et al., 2013; Lopez-Paz & Oquab, 2017; Bargiotas et al., 2021). As in most statistical problems, passing from the typical univariate to a multivariate setting is non-trivial. More precisely, carrying on multiple two-sample test will encounter the *Multiple Comparison Problem* (MCP), which refers to the fact that the probability of wrongly rejecting a set of null hypothesis (false positives, or Type-I error), in-

creases artificially with the number of tests. Standard MCP treatments include Bonferroni correction that scales the π -values by the number of hypotheses being tested (N) (Dunn, 1961), or non-parametric resampling test with a maximum statistic and permutation tests (Westfall & Young, 1992).

The *Multiple Two-Sample Testing* (MTST) problem appears in fields such as Spatial Statistics, Neuroscience, or Complex Systems. In these contexts, each test is associated with data sampled from a different ‘location’, and the validity of null hypotheses often depends on the ‘proximity’ between those locations. For instance, the Hebbian perspective stating “*Neurons that fire together wire together*” (Hebb, 1949) is common ground in Neuroscience, while Tobler’s *first law of Geography* (Tobler, 1970) eloquently stating “*Everything is related to everything else, but near things are more related than distant things*” is cornerstone in Spatial Statistics.

Multiple two-sample testing on graphs. Motivated by the above application fields, we study the particularly challenging problem of *graph-structured* MTST, where a TST is considered over each node $v \in V = \{1, \dots, N\}$ of a given fixed graph G , comparing two node-specific pdfs p_v and q_v . Then, the all N hypotheses are simultaneously tested:

$$\{H_{\text{null},v} : p_v = q_v \text{ vs. } H_{\text{alt},v} : p_v \neq q_v\}_{v \in V} \quad (1)$$

to determine $R_{\text{MT}} = \{v \in V \mid H_{\text{null},v} \text{ is found false}\}$, which contains the nodes with null hypotheses to be rejected with a given level of confidence $1 - \pi^{*1}$. The goal is for R_{MT} to be as close as possible to the set of hypotheses where really holds $p_v \neq q_v$, denoted by \mathbf{I}_0^c (i.e. the set complement of \mathbf{I}_0). As in any *Multiple Hypothesis Testing* (MT) approach, in this case determining R_{MT} requires three components:

1. A test statistic S_v for $H_{\text{null},v}$, estimated using the data of node v , to quantify the dissimilarity of p_v and q_v .
2. A π -value estimation framework to identify which of the $\{H_{\text{null},v}\}_{v \in V}$ to be rejected.
3. A Type-I error correction strategy to control the MCP.

In the context of graph-structured MTST, to the best of our knowledge, there exist mostly plug-in methods, in the sense that: they perform (1) and (2) independently for each node; then, for (3) they apply post-hoc Type-I error correction using an aggregation mechanism over the estimated π -values,

¹ p -values appear as π -values to distinguish them from pdf p .

¹Université Paris-Saclay, ENS Paris-Saclay, CNRS, Centre Borelli, France. Correspondence to: Alejandro de la Concha <alejandro.de_la_concha_duarte@ens-paris-saclay.fr>, Argyris Kalogeratos <argyris.kalogeratos@ens-paris-saclay.fr>.

or they avoid the MCP by defining a single test statistic from the multiple test statistics $\{S_v\}_{v \in V}$, and then estimate a π -value based on that quantity. The main drawback of these approaches is that individual test statistics that fail to quantify properly the difference between each pair of p_v and q_v may lead to inaccurate conclusions.

Notable graph-structured MT techniques include the *Permutation Cluster Test* (PCT) (Maris & Oostenveld, 2007), *Threshold-free Cluster Enhancement* (TFCE) (Smith & Nichols, 2009), and the *Structure-Adaptive Benjamini Hochberg Algorithm* (SAHBA) (Li & Barber, 2018), which assume that the null hypotheses to be rejected will be associated with a group of connected nodes. The π -values of PCT and TFCE procedures are estimated via a permutation test over a maximum test statistic. In contrast, SAHBA uses a reweighting mechanism of the node-level π -values, and relies on the assumption that connected nodes will show similar π -values.

Contribution. As a response to the above challenges, in this paper we present the *Collaborative Two-Sample Test* (CTST): a graph-structured TST built upon non-parametric methods and the notion of graph smoothness. Fig. 1 illustrates the approach. Distinct from existing works, CTST’s core novelty is that it not only *estimates jointly and in an associative manner* all node-level test statistics, but it also intertwines that estimation with the identification of the hypotheses to be rejected. Leveraging techniques from the ϕ -divergence estimation, Kernel Methods, Multitasking, and more specifically the GRULSIF framework (de la Concha et al., 2024). CTST adeptly quantifies the difference between p_v and q_v under minimal assumptions. Under the graph smoothness hypothesis, the collaborative estimation enforces the similarity of the test statistics S_u and S_v for connected nodes u and v . The induced regularity at the node-level test statistics is exploited by a permutation test that efficiently controls for the k -Family-Wise Error Rate (FWER), and identifies of nodes where $p_v \neq q_v$. Our experimental study using synthetic data and real seismic data, shows that CTST compares favorably against state-of-the-art Kernel-based techniques that disregard the geometry of the problem.

2. Preliminaries and problem statement

2.1. Preliminaries

General notations. Let a_i be the i -th entry of a vector a ; when the vector is itself indexed by j , we refer to its i -th entry by $a_{j,i}$. A_{ij} denotes the entry at the i -th row and j -th column of a matrix A , and $A_{i,:}$ is its i -th row. $\text{vec}(a_1, \dots, a_n)$ denotes the concatenation of the input vectors a_1, \dots, a_n in a single vector. $\mathbf{1}_M$ is a vector with M ones (resp. $\mathbf{0}_M$), I_M is a $M \times M$ identity matrix, and $\mathbb{1}\{\cdot\}$ is the indicator function.

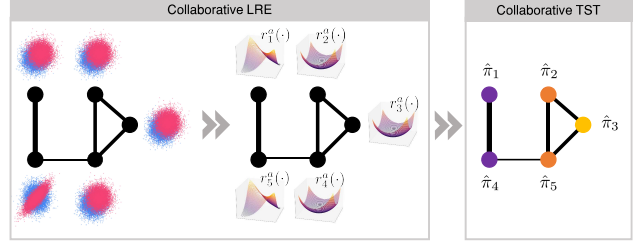


Figure 1: Collaborative multiple two-sample testing (CTST) based on collaborative LRE over a graph. **Left:** Given observations from two pdfs, p_v (blue) and q_v (pink) at each node v of a graph, GRULSIF estimates the associated relative likelihood-ratios $\{r_v^\alpha\}_v$ in a collaborative manner. In this example, it is easy to see how any given $x \in \mathcal{X} = \mathbb{R}^2$ gets essentially mapped to the graph signal $(r_1^\alpha(x), \dots, r_N^\alpha(x))^T$. **Right:** A visual summary of the CTST testing. The likelihood-ratios computed by GRULSIF are used to estimate node-level p -values $\hat{\pi}_v$ that allow us to eventually identify the nodes such that $p_v \neq q_v$.

The Euclidean norm and the dot product are denoted by $\|\cdot\|$ and $\langle \cdot, \cdot \rangle$. When those are endowed to a functional space \mathcal{F} , we write $\|\cdot\|_{\mathcal{F}}$ and $\langle \cdot, \cdot \rangle_{\mathcal{F}}$. For an observation x belonging to a d -dimensional input space, we write $x \in \mathcal{X} \subset \mathbb{R}^d$.

A fixed undirected weighted graph $G = (V, E, W)$ is defined by the set of N nodes V , and the set of edges E . Throughout the rest of the presentation, we suppose that the edges are positive-weighted and undirected, and that the nodes have no self-loops, i.e. the entries of its weight matrix $W \in \mathbb{R}^{N \times N}$ are such that $W_{uu} = 0, \forall u \in V$, and $W_{uv} = W_{vu} \geq 0$. In the rest, composite objects (vectors, matrices, sets, etc.) that refer to all the nodes of a graph, are denoted in bold font. Finally, the notion of *smoothness* is central in this work; the smoothness of a graph function $\vartheta : V \rightarrow \mathbb{R}$ over G is defined as $\sum_{(u,v) \in E} W_{uv} (\vartheta(u) - \vartheta(v))^2$. This notion generalizes for N estimates over the nodes of G , hence we use the umbrella term *graph smoothness* to refer to the expected behavior of a studied phenomenon over a graph, which in turn motivates the use of graph regularization techniques.

ϕ -divergences and likelihood-ratio. ϕ -divergences are non-negative functions measuring the dissimilarity between two probability measures. For two probability measures with pdfs p and q with respect to the Lebesgue measure, the ϕ -divergence comparing p and q is defined as:

$$\mathcal{D}_\phi(p||q) = \int \phi\left(\frac{q(x)}{p(x)}\right) p(x) dx, \text{ for } x \in \mathcal{X}, \quad (2)$$

where $\phi : \mathbb{R} \rightarrow \mathbb{R}$ is a convex and semi-continuous real function such that $\phi(1) = 0$ (Csiszár, 1967). Easy to see, $\mathcal{D}_\phi(p||q) = 0$ iff $p = q$. Moreover, as the integration in Eq. 2 is w.r.t. p , the output is more sensitive to points where p has higher mass, and hence ϕ -divergences may be non-symmetric functions, i.e. $\mathcal{D}_\phi(p||q) \neq \mathcal{D}_\phi(q||p)$.

The quantity $r(x) = \frac{q(x)}{p(x)}$ is called *likelihood-ratio* and is central in the computation of any ϕ -divergence. As we will see in Sec. 3.1, we can translate the approximation of the χ^2 -divergence between p and q to a likelihood-ratio estimation (LRE) problem. In practice, though, r may be an unbounded function, challenging non-parametric methods that may fail to converge. For this reason, a known workaround is to replace p by $p^\alpha(x) = (1-\alpha)p(x) + \alpha q(x)$, and use instead the α -relative likelihood-ratio function (Yamada et al., 2011): $r^\alpha(x) = \frac{q(x)}{p^\alpha(x)} \leq \frac{1}{\alpha}$, for any $0 \leq \alpha < 1$, $x \in \mathcal{X}$.

2.2. Problem statement

Let a fixed undirected and positive-weighted graph $G = (V, E, W)$, and suppose each node $v \in V$ has $n + n'$ (same for all nodes) iid observations from two unknown pdfs, p_v and q_v , respectively. The two data observations subsets taking values in the input space $\mathcal{X} \subset \mathbb{R}^d$ are:

$$\begin{cases} \mathbf{X} = \{\mathbf{X}_v\}_{v \in V} = \{\{x_{v,i} : x_{v,i} \stackrel{\text{iid}}{\sim} p_v\}_{i=1}^n\}_{v \in V}; \\ \mathbf{X}' = \{\mathbf{X}'_v\}_{v \in V} = \{\{x'_{v,i} : x'_{v,i} \stackrel{\text{iid}}{\sim} q_v\}_{i=1}^{n'}\}_{v \in V}. \end{cases} \quad (3)$$

The proposed CTST aims at solving the graph-structured multiple two-sample testing problem presented in Expr. 1. Fig. 1 presents an insightful visualization of the problem. In general terms, CTST comprises three steps:

1. *Collaborative estimation*: Joint estimation of the node-level relative likelihood-ratios, $\mathbf{r}^\alpha = (r_1^\alpha, \dots, r_N^\alpha)$, using the available data (Eq. 3). The vector-valued function \mathbf{r}^α is then used to approximate for each node v the χ^2 -divergence ($p_v \| q_v$).
2. *Node-level test statistics*: The ϕ -divergences' properties (see Sec. 2.1) make them good candidates for node-level test statistics. To deal with their non-symmetry, at each node the pair of node-level test statistics $\{S_v\}_{v \in V}$, $\{S'_v\}_{v \in V}$ are used, which corresponds to both the χ^2 -divergence ($p_v \| q_v$) and χ^2 -divergence ($q_v \| p_v$).
3. *π -value estimation*: A permutation test is used for the estimation of two sets of node-level π -values, $\{\pi_v\}_{v \in V}$ and $\{\pi'_v\}_{v \in V}$. These sets of π -values to identify the set of null hypotheses to be rejected (R_{CTST}). The permutation test guarantees weak control of FWER.

3. The proposed collaborative non-parametric two-sample test (CTST)

The foundation of the CTST method is the collaborative likelihood-ratio estimation (LRE) in a graph-structured setting. Conveniently for our purpose, this problem has been formally introduced in (de la Concha et al., 2024), and the *Graph-based Relative Unconstrained Least Squares Importance Fitting* (GRULSIF) method has been proposed, which we employ in this work. Before presenting the principal

components of CTST, we mention below basic notions regarding that non-parametric estimation.

Reproducing Kernel Hilbert Spaces. Given an input space $\mathcal{X} \subset \mathbb{R}^d$, we aim to estimate $r^\alpha(x)$ w.r.t. a Reproducing Kernel Hilbert Space (RKHS) \mathbb{H} containing as elements functions $f : \mathcal{X} \rightarrow \mathbb{R}$. \mathbb{H} is equipped with the inner product $\langle \cdot, \cdot \rangle_{\mathbb{H}} : \mathbb{H} \times \mathbb{H} \rightarrow \mathbb{R}$, which will be reproduced by a Mercer Kernel; i.e. by a continuous symmetric real function, which is the positive semi-definite kernel function $\mathbf{K}(\cdot, \cdot) : \mathcal{X} \times \mathcal{X} \rightarrow \mathbb{R}$. Then, the space \mathbb{H} enjoys the so-called RKHS reproducing property: $\langle \mathbf{K}(x, \cdot), f \rangle_{\mathbb{H}} = f(x)$, for any $f \in \mathbb{H}$; and also satisfies that $\mathbb{H} = \overline{\text{span}}(\{\mathbf{K}(x, \cdot) : \forall x \in \mathcal{X}\})$, where $\overline{\text{span}}$ refers to the closure of all the linear combinations of the elements $\mathbf{K}(x, \cdot) \in \mathbb{H}$, $\forall x \in \mathcal{X}$. Finally, the earlier seen concept of smoothness can be generalized in the RKHS: for $\vartheta(u), \vartheta(v) \in \mathbb{H}$, this is $\sum_{(u,v) \in E} W_{uv} \|\vartheta(u) - \vartheta(v)\|_{\mathbb{H}}^2$.

3.1. Step 1: Collaborative likelihood-ratio estimation

The graph-based framework for LRE (de la Concha et al., 2024) that we employ for this step, focuses on the χ^2 -divergence. By setting $\phi(r(x)) = \frac{(r(x)-1)^2}{2}$ in Eq. 2, one recovers the χ^2 -divergence (Pearson, 1900), $\mathcal{D}_\phi(p \| q) = PE(p \| q)$, which can be expressed as:

$$\begin{aligned} PE(p \| q) &:= \int \frac{(r(x)-1)^2}{2} p(x) dx & (4a) \\ &\geq \sup_{f \in \mathcal{F}} \int f(x) q(x) dx - \int \frac{f^2(x)}{2} p(x) dx - \frac{1}{2}, & (4b) \end{aligned}$$

where \mathcal{F} is a functional space. Ineq. 4b is known as the variational representation of the χ^2 -divergence, and it is a consequence of Lemma 1 in (Nguyen et al., 2008) that gives the conditions where such lower-bound is attained, i.e. when computing a ϕ -divergence amounts to solving an optimization problem in a functional space. In the case of χ^2 -divergence, the function f appearing in Ineq. 4b approximates the likelihood-ratio r .

As reasoned in Sec. 2.1, instead of estimating r , it is suggested to work with the relative likelihood-ratio r^α , hence to estimate $PE^\alpha(p \| q) := PE(p^\alpha \| q)$. Finally, we can express the variational representation of Ineq. 4b in expectation, using the data observations described in Expr. 3:

$$\begin{aligned} \mathbb{E}[PE(p^\alpha \| q)] &\geq \sup_{f \in \mathcal{F}} \mathbb{E}_{q(x')} [f(x')] - \frac{(1-\alpha)}{2} \mathbb{E}_{p(x)} [f^2(x)] \\ &\quad - \frac{\alpha}{2} \mathbb{E}_{q(x')} [f^2(x')] - \frac{1}{2}. \end{aligned} \quad (5)$$

The choice of the functional space \mathcal{F} is key for defining a learning algorithm that can be implemented in practice, and at the same time enjoying desired theoretical properties such as stability and consistency. In our approach, we opt for a RKHS whose geometry can enhance the graph smoothness

hypothesis. This derives from the fact that two functions $f_u, f_v \in \mathbb{H}$ close in the RKHS, will exhibit similarity when evaluated at the same point $x \in \mathcal{X}$, as elucidated below:

$$|f_u(x) - f_v(x)| = |\langle \mathbf{K}(x, \cdot), f_u - f_v \rangle_{\mathbb{H}}| \leq C \|f_u - f_v\|_{\mathbb{H}}, \quad (6)$$

where $0 < C < \infty$ is a constant so that $\sup_{x \in \mathcal{X}} \mathbf{K}(x, x) \leq C$. The first inequality is a consequence of the reproducing property of \mathbb{H} , and the second, is a consequence of the Cauchy-Schwarz inequality. Thus, enforcing graph smoothness, i.e. $\|f_u - f_v\|_{\mathbb{H}}$ to be small for two adjacent nodes u and v , is expected to lead to similar χ^2 -divergence estimates.

Optimization problem. The aim is to learn the vector-valued function $\mathbf{r}^\alpha = (r_1^\alpha, \dots, r_N^\alpha)$ via $\mathbf{f} = (f_1, \dots, f_N) \in \mathbb{H}^N$, where \mathbb{H} is a scalar RKHS. The cost function to optimize is:

$$\begin{aligned} \min_{\mathbf{f} \in \mathbb{H}^N} \frac{1}{N} \sum_{v \in V} & \left(\frac{(1-\alpha)}{2} \mathbb{E}_{p_v(x)} [f_v^2(x)] + \frac{\alpha}{2} \mathbb{E}_{q_v(x')} [f_v^2(x')] \right. \\ & \left. - \mathbb{E}_{q_v(x')} [f_v(x')] \right) + \frac{\lambda}{4} \sum_{u, v \in V} W_{uv} \|f_u - f_v\|_{\mathbb{H}}^2 + \frac{\lambda\gamma}{2} \sum_{v \in V} \|f_v\|_{\mathbb{H}}^2. \end{aligned} \quad (7)$$

The first term corresponds to the negative variational representation of the χ^2 -divergence at each node (i.e. the non-constant terms of Expr. 5). The second term evaluates the graph smoothness of the estimates. The last one is a penalty term that reduces the risk of overfitting (Sheldon, 2008).

Provided a dictionary $D_{\hat{L}}$ of \hat{L} basis functions, such that the finite dimensional space $\mathbf{F} = \text{span}(\{\varphi(x) : x \in D_{\hat{L}}\})$ approximates \mathbb{H} , it was further proposed to use Nyström approximation to replace the feature map $\varphi(x)$ by its orthogonal projection into the space \mathbf{F} . By determining a set of so-called *anchor points* in \mathbb{H} , $\varphi(x_1), \dots, \varphi(x_{\hat{L}})$, and via the associated kernel matrix, $\mathcal{K}_{\hat{L}} \in \mathbb{R}^{\hat{L} \times \hat{L}}$, $[\mathcal{K}_{\hat{L}}]_{ij} = \mathbf{K}(x_i, x_j)$, the new feature map derives:

$$\psi(\cdot) = \mathcal{K}_{\hat{L}}^{-\frac{1}{2}} (\mathbf{K}(\cdot, x_1), \dots, \mathbf{K}(\cdot, x_{\hat{L}}))^{\top}. \quad (8)$$

It was shown that, writing Problem 7 in terms of the empirical expectations and by involving the Nyström approximation, its solution $\hat{\mathbf{f}} = (\hat{f}_1, \dots, \hat{f}_N) \in \mathbb{H}^N$, takes the form:

$$\hat{f}_v(\cdot) = \psi(\cdot)^{\top} \hat{\theta}_v, \quad (9)$$

where $\hat{\theta}_v \in \mathbb{R}^{\hat{L}}$. By defining $\Theta = \text{vec}(\theta_1^{\top}, \dots, \theta_N^{\top})^{\top} \in \mathbb{R}^{N\hat{L}}$ that vectorizes all the node parameters, Problem 7 is rewritten as a quadratic problem over Θ :

$$\begin{aligned} \min_{\Theta \in \mathbb{R}^{N\hat{L}}} \frac{1}{N} \sum_{v \in V} & \left(\frac{(1-\alpha)}{2} \theta_v^{\top} H_{\psi, v} \theta_v + \frac{\alpha}{2} \theta_v^{\top} H'_{\psi, v} \theta_v - h'_{\psi, v} \theta_v \right) \\ & + \frac{\lambda}{4} \sum_{u, v \in V} W_{uv} \|\theta_v - \theta_u\|^2 + \frac{\lambda\gamma}{2} \sum_{v \in V} \|\theta_v\|^2, \end{aligned} \quad (10)$$

$$\begin{aligned} \text{where } H_{\psi, v} &= \frac{1}{n_v} \sum_{x \in \mathbf{X}_v} \psi(x) \psi(x)^{\top}, \quad h'_{\psi, v} = \frac{1}{n'_v} \sum_{x \in \mathbf{X}'_v} \psi(x), \\ H'_{\psi, v} &= \frac{1}{n'_v} \sum_{x \in \mathbf{X}'_v} \psi(x) \psi(x)^{\top}. \end{aligned} \quad (11)$$

Notice that $H_{\psi, v}, H'_{\psi, v} \in \mathbb{R}^{\hat{L} \times \hat{L}}$ and $h'_{\psi, v} \in \mathbb{R}^{\hat{L}}$.

Implementation. We follow the implementation of (de la Concha et al., 2024), which proposed to solve Problem 10 with the Cyclic Block Coordinate Descent (CBCD) (Beck & Tetruashvili, 2013; Li et al., 2018). If $n = n'$, then the final computational cost is $\mathcal{O}(N\hat{L}^3 + nN\hat{L}^2 + N\hat{L}^2 \log^2(N\hat{L}))$, where $\hat{L} \ll Nn$, which makes it scalable to real-life graphs. Other important implementation elements of GRULSIF, which we do not detail here, are the selection of the anchor points and the choice of the hyperparameters; the latter refers to the parameters of the kernel function $\mathbf{K}(\cdot, \cdot)$ and the regularization constants λ, γ . Since the regularization parameter α requires special attention, we provide several enlightening experiments for the studied CTST task in Appendix B.

3.2. Step 2: Node-level test statistics

After the parameter vector $\hat{\Theta}$ has been estimated, we can approximate the χ^2 -divergence ($p_v^\alpha \|q_v$) by:

$$\begin{aligned} PE^\alpha(p_v \|q_v) &:= PE(p_v^\alpha \|q_v) \\ &\approx h_{\psi, v}^{\top} \hat{\theta}_v - \frac{1-\alpha}{2} \hat{\theta}_v^{\top} H_{\psi, v} \hat{\theta}_v - \frac{\alpha}{2} \hat{\theta}_v^{\top} H'_{\psi, v} \hat{\theta}_v - \frac{1}{2} \\ &=: \hat{PE}_v^\alpha(\mathbf{X}_v \| \mathbf{X}'_v). \end{aligned} \quad (12)$$

To address the issue of the non-symmetry of divergence (see below Eq. 2), we identify the set of hypotheses to be rejected (R_{CTST}) by considering both the comparisons $PE^\alpha(p \|q)$ and $PE^\alpha(q \|p)$ to derive two sets of test statistics:

$$\begin{aligned} \{S_v\}_{v \in V} &= \{\hat{PE}_v^\alpha(\mathbf{X}_v \| \mathbf{X}'_v) \sim PE^\alpha(p_v \|q_v)\}_{v \in V}; \\ \{S'_v\}_{v \in V} &= \{\hat{PE}_v^\alpha(\mathbf{X}'_v \| \mathbf{X}_v) \sim PE^\alpha(q_v \|p_v)\}_{v \in V}. \end{aligned} \quad (13)$$

It has been shown that $\hat{PE}_v^\alpha(\mathbf{X}_v \| \mathbf{X}'_v)$ is an asymptotic unbiased estimator of $PE^\alpha(p_v \|q_v)$, and that the graph smoothness hypothesis and the collaborative LRE becomes more relevant as the estimation problem becomes more challenging (de la Concha et al., 2024), e.g. the fewer are the available observations per node. Notice, that the graph smoothness hypothesis would be totally satisfied if $\forall v \in V, p_v = q_v$, since all the relative likelihood-ratios will be equal to 1, hence $\|r_u^\alpha - r_v^\alpha\|_{\mathbb{H}} = 0$ for all connected nodes, u, v .

In this work, we exploit these properties of the collaborative LRE to propose a permutation test to control for FWER under the global hypothesis that for all nodes $p_v = q_v$ (H_{null}), but still sensitive enough to distinguish the nodes that experience a change of measure.

3.3. Step 3: π -value estimation

Our MT strategy applies a threshold η^* to each estimated node-level π -value $\{\hat{\pi}_v\}_{v \in V}$, hence considers the set of rejected hypotheses $R_{\text{MT}} = \{v \in V \mid \hat{\pi}_v < \eta^*\}$. We denote by $TP = \#\{v \mid v \in \mathbf{I}_0 \cap R_{\text{MT}}\}$ the number of true positives, and by $FP = \#\{v \mid v \in R_{\text{MT}} \setminus \mathbf{I}_0\}$ the number of false positives. We address the MCP by weak control of the k -Family-Wise Error Rate (FWER for $k = 1$), which is to control the probability to occur at least one false rejection of the individual node-level hypotheses:

$$\mathbb{P}(FP \geq 1 \mid \mathbf{I}_0) = \mathbb{P}(\{\exists v \in \mathbf{I}_0 : \hat{\pi}_v < \eta^*\}) \leq \pi^*, \quad (14)$$

where π^* is a user-defined rate (e.g. 0.01 or 0.05). Henceforth, we consider the following null hypothesis:

$$H_{\text{null}} : p_v = q_v, \forall v \in V. \quad (15)$$

Unlike *strong FWER control* that refers to any subset $\mathbf{I}_0 \subset V$, *weak FWER control* is less demanding as it deals only with the case where $\mathbf{I}_0 = V$.

Weak control in MTST is particularly relevant when studying the behavior of complex systems under two different experimental conditions. When there is no statistically significant difference between both conditions, then all nodes are expected to satisfy the null hypothesis (Expr. 15). Neuroscience offers a good example of this situation: several sensors are used to monitor brain activity, and MTST aims to detect clusters of firing neurons to a given stimulus. Classical methods, such as PCT (Maris & Oostenveld, 2007) and TFCE (Smith & Nichols, 2009), account for the inherent graph structure of the brain function and perform weak FWER control. By this, they mitigate the risk of claiming a false difference between two experimental conditions, while still maintaining the sensitivity necessary to detect true neural activity patterns.

The graph regularization introduced by the collaborative ϕ -divergence estimation of Step 1, leads to robust estimators against outliers in the node-level test statistics. This is particularly relevant under H_{null} and we want to avoid false positives, thus it is natural to exploit this feature and design a π -value estimation procedure with weak FWER control. Bear in mind that the flexibility of non-parametric LRE allows a certain level of heterogeneity of the pdfs in $\{p_v\}_{v \in V}$ and $\{q_v\}_{v \in V}$, as long as the relative likelihood-ratios of the pairs $((p_v, q_v)$ and (p_u, q_u) , $(u, v) \in E$) in adjacent nodes can be approximated by functions that are close in the shared RKHS. This feature complicates the distribution of the test statistic under H_{null} and, consequently, the derivation of an explicit formula for FWER control. Moreover, for the intended applications it is important to account for correlations between the node-level estimates.

We propose the use of a permutation test, which is a non-parametric strategy to address the above challenges with

Algorithm 1 – Collaborative two-sample tests over a graph (CTST)

- 1: **Input:** \mathbf{X}, \mathbf{X}' : two samples with observations over the graph $G = (V, E, W)$;
 - 2: $\alpha \in [0, 1)$: parameter of the relative likelihood-ratio;
 - 3: n_{perm} : the number of random permutations for π -value computation;
 - 4: π^* : the FWER rate for the test required by the user.
 - 5: **Output:** $\{\hat{\pi}_v\}_{v \in V}, \{\hat{\pi}'_v\}_{v \in V}$: a pair of π -values for each node;
 - 6: R_{CTST} : nodes where the null hypothesis $H_{\text{null}, v} : p_v = q_v$ is rejected.
-
- 7: Compute the anchor points associated with the kernel $K : \mathcal{X} \times \mathcal{X} \rightarrow \mathbb{R}$ (see \star)
 - 8: Select the hyperparameters $\sigma_1^*, \lambda_1^*, \gamma_1^*, \sigma_2^*, \lambda_2^*, \gamma_2^*$ (see \star)
 - 9: Estimate $\hat{\Theta}_1(\mathbf{X}, \mathbf{X}') = \text{GRULSIF}(\mathbf{X}, \mathbf{X}', \alpha, \sigma_1^*, D_1, \gamma_1^*, \lambda_1^*)$
 $\hat{\Theta}_2(\mathbf{X}', \mathbf{X}) = \text{GRULSIF}(\mathbf{X}', \mathbf{X}, \alpha, \sigma_2^*, D_2, \gamma_2^*, \lambda_2^*)$
 - 10: Compute $S_v = \{\hat{P}E_v^\alpha(X_v, X'_v)\}_{v \in V}$ and $S'_v = \{\hat{P}E_v^\alpha(X'_v, X_v)\}_{v \in V}$
 using $\hat{\Theta}_1(\mathbf{X}, \mathbf{X}')$, $\hat{\Theta}_2(\mathbf{X}', \mathbf{X})$ (see Expr. 12)
 - 11: **Permutation test**
 - 12: **for** $i \in \{1, \dots, n_{\text{perm}}\}$ **do**
 - 13: Generate a random permutation τ of the set such that
 $\mathbf{X}^{(\tau)} = \{X_{\cdot, \tau(1)}, \dots, X_{\cdot, \tau(n+n')}\}$
 - 14: Assign the first n elements of $\mathbf{X}^{(\tau)}$ to the set $\hat{\mathbf{X}}$ and the rest n' to the $\hat{\mathbf{X}}'$
 - 15: Compute $\hat{\Theta}_1(\hat{\mathbf{X}}, \hat{\mathbf{X}}')$ and $\hat{\Theta}_2(\hat{\mathbf{X}}', \hat{\mathbf{X}})$
 - 16: Compute $\{\hat{P}E_v^\alpha(\hat{\mathbf{X}}_v, \hat{\mathbf{X}}'_v)\}_{v \in V}$ and $\{\hat{P}E_v^\alpha(\hat{\mathbf{X}}'_v, \hat{\mathbf{X}}_v)\}_{v \in V}$
 using $\hat{\Theta}_1(\hat{\mathbf{X}}, \hat{\mathbf{X}}')$, $\hat{\Theta}_2(\hat{\mathbf{X}}', \hat{\mathbf{X}})$
 - 17: Compute the test statistic $s_1^i = \max_v \{\hat{P}E_v^\alpha(\hat{\mathbf{X}}_v, \hat{\mathbf{X}}'_v)\}_{v \in V}$
 and $s_2^i = \max_v \{\hat{P}E_v^\alpha(\hat{\mathbf{X}}'_v, \hat{\mathbf{X}}_v)\}_{v \in V}$
 - 18: **end for**
 - 19: **for** $v \in \{1, \dots, N\}$ **do**
 - 20: $\hat{\pi}_v = \frac{1}{n_{\text{perm}}} \sum_{i=1}^{n_{\text{perm}}} \mathbb{1}\{S_v \leq s_1^i\}$
 - 21: $\hat{\pi}'_v = \frac{1}{n_{\text{perm}}} \sum_{i=1}^{n_{\text{perm}}} \mathbb{1}\{S'_v \leq s_2^i\}$
 - 22: **end for**
 - 23: **Identify the nodes where the null hypothesis should be rejected**
 - 24: Define the set $R_{\text{CTST}} = \{v \in V \mid \hat{\pi}_v \leq \frac{\pi^*}{2} \text{ or } \hat{\pi}'_v \leq \frac{\pi^*}{2}\}$
 - 25: **return** $\{\hat{\pi}_v\}_{v \in V}, \{\hat{\pi}'_v\}_{v \in V}, R_{\text{CTST}}$

\star Steps 7 & 8 are treated using the implementation of (de la Concha et al., 2024).

out restricting our framework (Westfall & Young, 1992). The designed permutation test is over the vectors $X_{\cdot, j} = (x_{1,j}, \dots, x_{N,j})^\top$ (resp. $X'_{\cdot, j} = (x'_{1,j}, \dots, x'_{N,j})^\top$), each one carrying the observations having a given sample index j for all nodes. The permutation test infers the distribution of the maximum test statistic $S_G = \max_{v \in V} S_v$, and uses it to determine R_{CTST} , achieving this way weak FWER control at the level of π^* 's.

The complete CTST algorithm is provided in Alg. 1. Theorem 3.1 validates that CTST is a MT procedure with weak FWER control, provided a user-defined rate π^* . The technical details of the proof are provided in Appendix A.

Theorem 3.1. *Consider Problem 1 and assume the observations $\mathbf{X} = \{X_v\}_{v \in V}$ are iid for each node $v \in V$, same for and $\mathbf{X}' = \{X'_v\}_{v \in V}$ (see Eq. 3). Let $\hat{\mathbf{X}}, \hat{\mathbf{X}}'$ the permuted datasets as described in Alg. 1 and π^* a user-defined rate. Let $F(\cdot \mid \mathbf{X} \cup \mathbf{X}')$ denote the probability distribution of $S(\hat{\mathbf{X}} \parallel \hat{\mathbf{X}}') = \max_{v \in V} \hat{P}E_v^\alpha(\hat{X}_v \parallel \hat{X}'_v)$ given $\mathbf{X} \cup \mathbf{X}'$ and let $\hat{q}(\mathbf{X} \cup \mathbf{X}') = \sup\{s \in \mathbb{R} \mid F(s \mid \mathbf{X} \cup \mathbf{X}') \leq 1 - \frac{\pi^*}{2}\}$ be the point determining the upper $((1 - \frac{\pi^*}{2}) \cdot 100)$ -percentile. Then, if H_{null} is true, that is $p_v = q_v, \forall v \in V$, then it holds:*

$$\mathbb{P}(S > \hat{q}'(\mathbf{X} \cup \mathbf{X}')) \leq \frac{\pi^*}{2}. \quad (16)$$

Moreover, when $S' = \max_{v \in V} \hat{F}E_v^\alpha(\hat{X}'_v \| \hat{X}_v)$ is used as a test statistic, then, under H_{null} we have:

$$\mathbb{P}(S > \hat{q}(\mathbf{X} \cup \mathbf{X}')) \text{ or } S' > \hat{q}'(\mathbf{X} \cup \mathbf{X}') \leq \pi^*, \quad (17)$$

which implies $\text{FWER}(R_{\text{CTST}}) = \mathbb{P}(FP \geq 1 | H_{\text{null}}) \leq \pi^*$.

3.4. A CTST variant ignoring the graph structure

We can derive a reduced CTST variant relying on POOL, which is a GRULSIF variant that makes use of the same estimation framework, but neutralizes the graph component (i.e. by setting $W = \mathbf{0}_{N \times N}$ in Eq. 10) (de la Concha et al., 2024). This POOL-CTST variant can be relevant when there is no graph underlying the MT problem. Note that POOL can be seen as a variant of RULSIF (Yamada et al., 2011; 2013), while differing to the fact that: i) its joint hyperparameter selection for all nodes based on the mean score $\frac{1}{N} \sum_{v \in V} \left(\frac{1-\alpha}{2} \theta_v^T H_{\psi, v} \theta_v + \frac{\alpha}{2} \theta_v^T H'_{\psi, v} \theta_v - h'_{\psi, v} \theta_v \right)$, compared to RULSIF's independent hyperparameter selection for each node; ii) it uses the Nyström dimensionality reduction technique over all the full data observations, while RULSIF uses a simple uniform random subsampling at each node or all the data (Sugiyama et al., 2012).

4. Experiments

CTST is put in action in the context of graph-structured MT, in synthetic and real scenarios. The goal is to show the gains of combining a non-parametric graph-based collaborative estimation of node-level test statistics, with the weak FWER control based on permutation test with a maximum statistic. Note that CTST is not a direct competitor to methods such as SAHBA, PCT, or TFCE (see Sec. 1). In fact, those can be seen as complementary approaches to CTST, as they could post-process CTST's output. Studying how to combine these approaches is beyond the scope of this paper.

To make fair comparisons and keep the flexibility of non-parametric methods, we restrict our attention to estimation approaches built upon Kernel Methods. We compare against LRE-based non-parametric algorithms, where the test statistics correspond to ϕ -divergence estimates, and against kernel-based methods built upon MMD (Gretton et al., 2012), which is the state-of-the-art in non-parametric statistical testing. Tab. 1 shows all the compared methods and that only CTST integrates a graph structure.

Each non-parametric method requires fixing the regularization constants and the hyperparameters of the kernel function; we focus on Gaussian kernels with width parameter σ . LRE-based methods use cross-validation to fix the hyperparameters, while from several works addressing this issue for MMD, we compare against the original MMD-MEDIAN version that is based on the median heuristic (Gretton et al., 2012), and the MMD-MAX method proposed in (Suther-

land et al., 2017) that aims at a score associated with the power of the two-sample test. Details on hyperparameter selection are provided in Appendix B.

For the competitors, we follow the traditional MT approach: we first estimate node-level test statistics independently for each node, and then we control for the MCP using a non-parametric resampling test with a maximum statistic (Westfall & Young, 1992), which achieves weak FWER control. The node-level test statistics $\{S_v\}_{v \in V}$ coincide with the notion of dissimilarity measured by each method (ϕ -divergence or MMD), and the distribution of $S_G = \max_{v \in V} S_v$ under the H_{null} is estimated via a permutation test (see Alg. 1). We address the non-symmetry of the ϕ -divergence-based methods same as we did in Sec. 3.2 for CTST, by comparing both p, q and q, p . Then, given a user-provided threshold rate π^* , we identify the sets of rejected hypotheses $R_{\phi\text{-div}} = \{v \in V | \hat{\pi}_v < \frac{\pi^*}{2} \text{ or } \hat{\pi}'_v < \frac{\pi^*}{2}\}$ and $R_{\text{MMD}} = \{v \in V | \hat{\pi}_v < \pi^*\}$.

Each instance of the four designed fully synthetic scenarios is generated by first generating a random graph and then by defining the scheme of the occurring change over a subset of the nodes.

- *Synth.Ia&b* use a *Stochastic Block Model* (SBM) with 4 clusters, with 25 nodes each (intra-cluster edge probability: 0.5; inter-cluster edge probability: 0.01). Then, a cluster-based scheme sets the same behavior (change of measure or not) for all the nodes of each cluster, C_1, \dots, C_4 .

- *Synth.IIa&b* use a *Grid* graph (GRID) with 100 nodes forming a 10×10 regular tiling. In this case, an ego-network-based scheme is employed, which picks a node u at random, with probability proportional to its node degree, and then considers that only the nodes in u 's 2-hop ego-network, denoted simply as $C(u)$, shall experience a change of measure.

4.1. Synthetic experiments

Synthetic scenarios provide by design the set $\mathbf{I}_0^0 = V \setminus \mathbf{I}_0$, which is the indexes v 's where $p_v \neq q_v$, hence allow the comparison of the power of the different MT frameworks. The scenarios detailed in Tab. 2 are similar to those in (de la Concha et al., 2024) to satisfy the graph smoothness hypothesis (connected nodes have similar behavior), and to pose various challenges to the LRE addressed by GRULSIF. On the top of each of those scenarios, we build a two-sample test comparing p_v vs. q_v . The two pdfs may differ in terms of mean, shape, covariance, etc. (see the node-level hypotheses in Tab. 2). Moreover, there can be more than one type of change in the same scenario.

We measure the performance of a MT procedure along two axes: First, the efficiency of its FWER control, i.e. the probability to occur one or more false positives under the H_{null} of Eq. 15. Second, how informative the estimated node-level π -values are, i.e. whether the low π -values are

Table 1: List of competitors. All the methods that are included in our experimental evaluation study for the graph-structured multiple two-sample test problem. l.-r. indicates the method that estimates the non-regularized likelihood-ratio ($\alpha = 0$).

Method	Reference	Estimate	Similarity measure	Graph
KLIEP	(Sugiyama et al., 2007)	l.-r.	KL-divergence	No
LSTT	(Sugiyama et al., 2011b)	l.-r.	χ^2 -divergence	No
RULSIF	(Yamada et al., 2013)	relative l.-r.	χ^2 -divergence	No
MMD	(Gretton et al., 2012)	MMD	MMD	No
POOL	this work (Sec. 3.4)	relative l.-r.	χ^2 -divergence	No
CTST	this work	relative l.-r.	χ^2 -divergence	Yes

Table 2: Synthetic experiments. The scenarios are defined by the graph structure they employ and the node-level distributions (p_v and q_v) generating the data observations at each node. • denotes cases where distributions or their parameters remain unchanged.

Experiment	Location	Node-level hypotheses	
		p_v	q_v
Synth.Ib SBM 4 clusters	$v \in C_1$	$N(\mu=0, \sigma=1)$	vs. Uniform($-\sqrt{3}, \sqrt{3}$)
	$v \in C_2 \cup C_3$	$N(\mu=0, \sigma=1)$	vs. •
	$v \in C_4$	$N(\mu=0, \sigma=1)$	vs. $N(\mu=1, \sigma=0.5)$
Synth.Ib SBM 4 clusters	$v \in C_1 \cup C_2$	$N(\mu=(0,0)^T, \Sigma_{1,2}=-\frac{1}{2})$	vs. •
	$v \in C_3$	$N(\mu=(0,0)^T, \Sigma_{1,2}=\frac{1}{2})$	vs. $N(\mu=0, \Sigma_{1,2}=0)$
	$v \in C_4$	$N(\mu=(0,0)^T, \Sigma_{1,2}=0)$	vs. $N(\mu=(1,1)^T, \Sigma_{1,2}=0)$
Synth.IIa GRID 10x10	$v \in C(u)$	$N(\mu=0, \Sigma_{i,i}=1, \Sigma_{1,2}=\frac{1}{2}, \Sigma_{3,1}=0)$	vs. $N(\mu=0, \Sigma_{i,i}=0.5, \Sigma_{1,2}=0, \Sigma_{3,1}=0)$
	$v \notin C(u)$	$N(\mu=0, \Sigma_{i,i}=1, \Sigma_{1,2}=\frac{1}{2}, \Sigma_{3,1}=0)$	vs. •
Synth.IIb GRID 10x10	$v \in C(u)$	$N(\mu=(0,0)^T, \Sigma=10I_2)$	vs. Gaussian Mixture (with equal proportion) $N(\mu_1=(0,0)^T, \Sigma=5I_2)$ $N(\mu_2=(0,5)^T, \Sigma=5I_2)$ $N(\mu_3=(0,-5)^T, \Sigma=5I_2)$ $N(\mu_4=(5,0)^T, \Sigma=5I_2)$ $N(\mu_5=(-5,0)^T, \Sigma=5I_2)$
	$v \notin C(u)$	$N(\mu_1=(0,0)^T, \Sigma=10I_2)$	vs. •

associated with nodes in \mathbf{I}_0^c . From a practitioner’s perspective, when comparing a complex system across two different time-stamps or experimental conditions, methods that are robust to false positives (avoid asserting a non-existent statistically significant difference) are preferred. Second, we measure how accurately the MT procedure identifies the nodes responsible for an observed deviation. This quality is summarized by the Alternative Free-response Receiver-Operating Characteristic (AFROC) curve (Chakraborty & Winter, 1990). The detailed estimation we used for the AFROC curves is provided in Appendix B.

The AUC of the AFROC curves is reported in Tab. 3. The higher the value of the AUC the better, indicating that a method achieved the required FWER level of $\pi^* = 0.05$ and is still able to identify the nodes in \mathbf{I}_0^c . The AFROC curves we designed ignore the false positives at nodes $\{v | v \in R_{\text{MT}} \setminus \mathbf{I}_0\}$. For this reason, we report also the AUC of the ROC curves. The interpretation should take AFROC-AUC as the most important criterion, and ROC-AUC rather as a tiebreaker for approaches with similar AFROC-AUC.

Findings. Tab. 3 shows that CTST is a clearly more efficient test compared to the rest of the methods that disregard the geometry of the problem. The role of the graph becomes more relevant as the observations are fewer, and when the difference between p_v and q_v is more subtle. This effect is more evident when comparing CTST to the no-graph variant POOL (Sec. 3.4). An additional advantage of CTST over POOL is that it is robust and consistent when varying the

Table 3: Results on synthetic scenarios. Non-parametric methods applied on multiple two-sample testing over a known graph. Keeping the graph fixed, the AFROC and ROC curves were computed over 1000+1000 experiment instances generated over H_{null} and H_{alt} of Problem 1, respectively. Higher AUC values are better.

Experiment	Method	$n = n' = 50$		$n = n' = 100$		$n = n' = 250$	
		AFROC AUC	ROC AUC	AFROC AUC	ROC AUC	AFROC AUC	ROC AUC
Synth.Ia	CTST $\alpha=0.1$	0.50	0.93	0.66	0.99	0.99	1.00
	POOL $\alpha=0.1$	0.28	0.84	0.49	0.93	0.64	0.99
	RULSIF $\alpha=0.1$	0.18	0.88	0.47	0.76	0.76	1.00
	LSTT	0.07	0.84	0.38	0.91	0.23	0.76
	KLIEP	0.00	0.74	0.34	0.89	0.55	1.00
	MMD-MEDIAN	0.33	0.82	0.50	0.89	0.54	0.97
MMD-MAX	0.33	0.82	0.50	0.88	0.54	0.97	
Synth.Ib	CTST $\alpha=0.1$	1.00	1.00	1.00	1.00	1.00	1.00
	POOL $\alpha=0.1$	0.72	1.00	0.99	1.00	1.00	1.00
	RULSIF $\alpha=0.1$	0.44	0.97	0.88	0.88	0.94	0.95
	LSTT	0.36	0.94	0.77	0.90	0.96	0.96
	KLIEP	0.33	0.90	0.79	0.94	0.92	0.93
	MMD-MEDIAN	0.48	0.96	0.52	0.99	0.96	1.00
MMD-MAX	0.48	0.96	0.52	0.99	0.96	1.00	
Synth.IIa	CTST $\alpha=0.1$	0.94	1.00	1.00	1.00	1.00	1.00
	POOL $\alpha=0.1$	0.18	0.98	0.22	0.84	1.00	1.00
	RULSIF $\alpha=0.1$	0.01	0.82	0.30	0.99	0.52	0.61
	LSTT	0.00	0.81	0.23	0.83	0.97	1.00
	KLIEP	0.00	0.80	0.29	0.91	0.67	0.73
	MMD-MEDIAN	0.00	0.81	0.01	0.95	0.43	1.00
MMD-MAX	0.00	0.82	0.01	0.95	0.39	1.00	
Synth.IIb	CTST $\alpha=0.1$	0.30	0.92	0.65	0.98	0.98	1.00
	POOL $\alpha=0.1$	0.02	0.84	0.12	0.95	0.78	1.00
	RULSIF $\alpha=0.1$	0.01	0.80	0.06	0.92	0.75	1.00
	LSTT	0.00	0.78	0.04	0.91	0.66	1.00
	KLIEP	0.00	0.79	0.03	0.85	0.63	1.00
	MMD-MEDIAN	0.00	0.78	0.05	0.92	0.60	1.00
MMD-MAX	0.00	0.78	0.05	0.92	0.52	1.00	

regularization parameter α (see Appendix B).

4.2. Two-sample testing on real seismic data

We use seismic data as a practical example showcasing CTST’s potential in performing spatial statistical analyses. We remark, though, that this should not be interpreted as an attempt to outperform existing state-of-the-art methods in that field. Geological hazard monitoring systems comprises of several stations strategically positioned across a territory to monitor ground noise and shaking through a number of sensors. When a seismic event occurs, it travels through the earth, and this is captured by the monitoring sensors. Stations closer to the epicenter of a seism tend to show higher response to the event, exhibiting faster reactions and more pronounced differences in their pre- and post-event data. In this context, a graph-structured multiple two-sample test can be used for assessing the significance of a seismic event, and for identifying the stations and time periods during which each of them got activated.

Data preprocessing: We analyze two seismic events occurred in New Zealand: Seism A is of magnitude 5.5 in Richter scale, occurred on May 31, 2021²; Seism B is a weaker seism of magnitude 2.6, occurred on Oct 2, 2023³. The stations are equipped with strong-motion accelerome-

²The data are publicly available by the GeoNet project (GNS Science, 1970): <https://www.geonet.org.nz/earthquake/2021p405872>

³<https://www.geonet.org.nz/earthquake/2023p741652>

ters that provide 3d signals corresponding to the shaking across three perpendicular directions. To compare the situation before and after an event, we analyze the waveforms from 50 seconds before to 50 seconds after the event, at 100 Hz frequency. The preprocessing details are in Appendix B.

Graph structure: We build in two steps a graph representation that accounts for both spatial and temporal similarities between the seismic stations and their signals. The first step is to build an unweighted *spatial graph* $G_S = (V, E, W)$ considering as nodes the stations whose all accelerometers have available data at the analyzed time period. Edges are drawn from each station to its geographical 3-nearest-neighbors. Subsequently, we integrate the temporal dimension by building a *multiplex graph* $G_{S \times T}$ over G . We segment the signal before and after the seismic event in 10 time-windows, each containing the same amount of observations. $G_{S \times T}$ indexes the nodes of G_S by the time-window, $V \times \mathcal{T}$, where $\mathcal{T} = \{1, \dots, 10\}$. Two nodes in $G_{S \times T}$, (u, t) and (v, t') , are connected: i) if $t = t'$ and $(u, v) \in E$, i.e. they refer to the same time-window and the nodes u and v are connected in the spatial graph G_S , ii) or if $u = v$ and $|t' - t| = 1$, i.e. each node $v \in V$ is connected to its ‘copies’ in the two adjacent time-windows.

The data observations are indexed by the node and the time-window they belong, so the pdfs $\{p_{(v,t)}\}_{(v,t) \in V \times T}$ and $\{q_{(v,t)}\}_{(v,t) \in V \times T}$. After the preprocessing, we obtain two samples for each pair (v, t) , $X_{(v,t)} = \{x_{((v,t),i)}\}_{i=1}^{100} \sim p_{(v,t)}$ and $X'_{(v,t)} = \{x'_{((v,t),i)}\}_{i=1}^{100} \sim q_{(v,t)}$. We denote by $t = 0$ the beginning of the sample, that is 50 seconds before the seism. Then, the set $X_{(v,1)}$ refers to the first 5 seconds of preprocessed observations after $t = 0$ and $X'_{(v,1)}$ the 5 seconds of preprocessed observations after the event. Under this configuration, a two-sample test aims to identify the pairs (v, t) where $p_{(v,t)} \neq q_{(v,t)}$. For each method, a figure shows the map of the computed π -values, where the nodes (v, t) whose π -values is smaller than 0.05 are highlighted. We only report the largest cluster of $C_{S \times T}$ of $G_{S \times T}$, containing such nodes.

Findings. Fig. 2 shows a visual of the CTST result for Seism A, while the visualization of the rest of the results are in Appendix B.2.3. All the tested methods detect correctly an occurring seismic event and identify the most sensitive nodes as those closer to the epicenter. However, the methods that do not account the graph structure, which here encodes the expected spatial and temporal similarities between stations, lead to results where detections seem not informative. For example, looking at the associated π -values, the effect of a seism takes longer to fade out even when it ceases to be visible in the signals. Contrary, CTST recovers most of the nodes closer to the epicenter and follows better the evolution of the seismic event. These findings are compatible with the results found in the synthetic experiments, as the

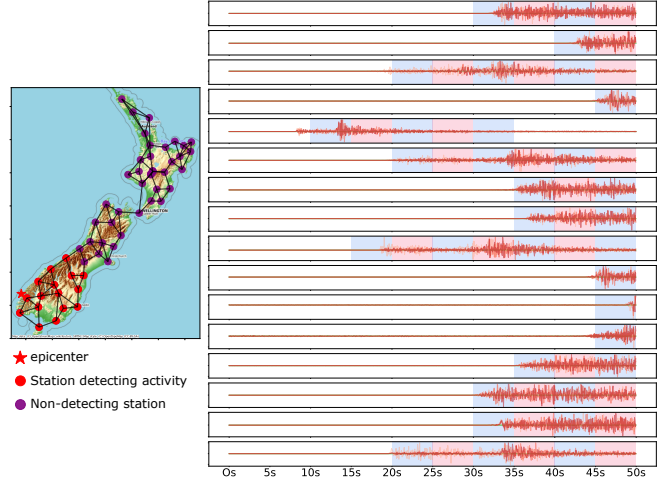


Figure 2: Seism A. Result of the proposed graph-based CTST (with $\alpha = 0.1$). **Left:** The location of the stations on the map of New Zealand connected in a 3NN graph. **Right:** The post-event signals associated with the stations (in proximity order to the epicenter) detecting activity in at least one time-window (colored).

AFROC-AUC and ROC-AUC measures show that CTST is more robust to false alarms, and that it recovers the nodes of interest with a higher confidence when the assumption of graph smoothness of the likelihood-ratios is satisfied.

5. Conclusions and further work

In this paper, we introduced a novel graph-structured non-parametric test designed for multiple two-sample testing over the nodes of a graph. Its appeal is that it integrates advances in collaborative likelihood-ratio estimation to compute jointly node-level test statistics and identify null hypotheses to be rejected, under a graph smoothness hypothesis. This approach is flexible and capable of dealing with complex scenarios in which the data at every node can be multivariate, the nature of the difference between the compared pdfs is unknown and it is allowed a certain amount of heterogeneity among the tests of the nodes. Synthetic and real experiments show that our methods compare favorably against state-of-the-art non-parametric approaches that do not account for the similarity between tests. As future work, it would be interesting to extend the use of this approach to more applications, and design strategies for stricter Type-I error control.

References

Bargiotas, I., Kalogeratos, A., Limnios, M., Vidal, P.-P., Ricard, D., and Vayatis, N. Revealing posturographic profile of patients with parkinsonian syndromes through a novel hypothesis testing framework based on machine learning. *PLOS ONE*, 16(2), 02 2021.

Beck, A. and Tetrushvili, L. On the convergence of block coordi-

- nate descent type methods. *SIAM Journal on Optimization*, 23: 2037–2060, 2013.
- Beyreuther, M., Barsch, R., Krischer, L., Megies, T., Behr, Y., and Wassermann, J. ObsPy: A Python Toolbox for Seismology. *Seismological Research Letters*, 81(3):530–533, 05 2010.
- Chakraborty, D. P. and Winter, L. H. Free-response methodology: alternate analysis and a new observer-performance experiment. *Radiology*, 174(3):873–881, March 1990.
- Chen, Y., Wang, T., and Samworth, R. High-dimensional, multi-scale online changepoint detection. *Journal of Royal Statistical Society, Ser. B., to appear*, 2021.
- Csiszár, I. On topological properties of f-divergences. *Studia Scientiarum Mathematicarum Hungarica*, 2:329—339, 1967.
- de la Concha, A., Vayatis, N., and Kalogeratos, A. Online non-parametric likelihood-ratio estimation by Pearson-divergence functional minimization, 2023.
- de la Concha, A., Kalogeratos, A., and Vayatis, N. Collaborative likelihood-ratio estimation over graphs, 2024.
- Dunn, O. J. Multiple comparisons among means. *Journal of the American Statistical Association*, 56(293):52–64, 1961.
- GNS Science. GeoNet Aotearoa New Zealand Earthquake Catalogue, 1970.
- Gretton, A., Borgwardt, K. M., Rasch, M. J., Schölkopf, B., and Smola, A. A kernel two-sample test. *Journal of Machine Learning Research*, 13(25):723–773, 2012.
- Harchaoui, Z., Bach, F., Cappe, O., and Moulines, E. Kernel-based methods for hypothesis testing: A unified view. *IEEE Signal Processing Magazine*, 30(4):87–97, 2013. doi: 10.1109/MSP.2013.2253631.
- Hebb, D. O. *The organization of behavior: A neuropsychological theory*. Wiley, New York, June 1949.
- Li, A. and Barber, R. F. Multiple Testing with the Structure-Adaptive Benjamini–Hochberg Algorithm. *Journal of the Royal Statistical Society Series B: Statistical Methodology*, 81(1):45–74, 11 2018.
- Li, X., Zhao, T., Arora, R., Liu, H., and Hong, M. On faster convergence of cyclic block coordinate descent-type methods for strongly convex minimization. *Journal of Machine Learning Research*, 18(184):1–24, 2018.
- Lopez-Paz, D. and Oquab, M. Revisiting classifier two-sample tests. In *Int. Conf. on Learning Representations*, 2017.
- Maris, E. and Oostenveld, R. Nonparametric statistical testing of EEG- and MEG-data. *Journal of Neuroscience Methods*, 164(1):177–190, August 2007.
- Nguyen, X., Wainwright, M. J., and Jordan, M. Estimating divergence functionals and the likelihood ratio by penalized convex risk minimization. In *Advances in Neural Information Processing Systems*, 2008.
- Pearson, K. X. On the criterion that a given system of deviations from the probable in the case of a correlated system of variables is such that it can be reasonably supposed to have arisen from random sampling. *The London, Edinburgh, and Dublin Philosophical Magazine and Journal of Science*, 50(302):157–175, 1900.
- Sheldon, D. Graphical Multi-Task Learning. Technical report, Cornell University, 2008.
- Smith, S. and Nichols, T. Threshold-free cluster enhancement: Addressing problems of smoothing, threshold dependence and localisation in cluster inference. *NeuroImage*, 44(1):83–98, January 2009.
- Sugiyama, M., Nakajima, S., Kashima, H., Buenau, P., and Kawanabe, M. Direct importance estimation with model selection and its application to covariate shift adaptation. In *Advances in Neural Information Processing Systems*, volume 20, 2007.
- Sugiyama, M., Suzuki, T., Itoh, Y., Kanamori, T., and Kimura, M. Least-squares two-sample test. *Neural networks : the official journal of the International Neural Network Society*, 24:735–51, 04 2011a.
- Sugiyama, M., Suzuki, T., Itoh, Y., Kanamori, T., and Kimura, M. Least-squares two-sample test. *Neural Networks*, 24(7): 735–751, 2011b.
- Sugiyama, M., Suzuki, T., and Kanamori, T. *Density Ratio Estimation in Machine Learning*. Cambridge University Press, 2012.
- Sutherland, D. J., Tung, H.-Y., Strathmann, H., De, S., Ramdas, A., Smola, A., and Gretton, A. Generative models and model criticism via optimized maximum mean discrepancy. In *Int. Conf. on Learning Representations*, 2017.
- Tobler, W. R. A computer movie simulating urban growth in the detroit region. *Economic Geography*, 46:234–240, 1970.
- Westfall, P. H. and Young, S. S. *Resampling-based multiple testing*. Wiley Series in Probability and Statistics. John Wiley & Sons, Nashville, TN, December 1992.
- Yamada, M., Suzuki, T., Kanamori, T., Hachiya, H., and Sugiyama, M. Relative density-ratio estimation for robust distribution comparison. In *Advances in Neural Information Processing Systems*, 2011.
- Yamada, M., Suzuki, T., Kanamori, T., Hachiya, H., and Sugiyama, M. Relative density-ratio estimation for robust distribution comparison. *Neural Computation*, 25(5):1324–1370, 2013.

A. Regarding CTST and FWER control

Bellow, we provide the proof for Theorem 3.1, which validates that CTST achieves weak FWER control.

Proof of Theorem 3.1. We start with the assumption that the observations of \mathbf{X} come from the joint pdf \mathbf{p} , whose marginals are the node pdfs $\{p_v\}_{v \in V}$. Same for those observations of \mathbf{X}' collected from the joint pdf \mathbf{q} whose marginals are the node pdfs $\{q_v\}_{v \in V}$. We assume the observations at a specific node v , namely $\{x_{v,i}\}_{v \in V, i=1, \dots, n}$ and $\{x'_{v,i}\}_{v \in V, i=1, \dots, n'}$, are iid over the variation of index i . Let us define the set of vectors as $\mathbf{Z} = \{Z_1, Z_2, \dots, Z_{n+n'}\}$, where $Z_i = X_{:,i} = \{x_{v,i}\}_{v \in V}$ for $i \in \{1, \dots, n\}$ and $Z_{n+j} = X'_{:,j} = \{x'_{v,j}\}_{v \in V}$ for $j \in \{1, \dots, n'\}$. Then, under H_{null} and the hypothesis of statistical independence, we have that the probability distribution \mathbf{p}^z is exchangeable, where exchangeability means that for any permutation τ on $\{1, \dots, n+n'\}$, the permuted set of vectors $\mathbf{Z}_\tau = \{Z_{\tau(1)}, Z_{\tau(2)}, \dots, Z_{\tau(n+n')}\}$ follow the same law \mathbf{p}^z .

Given a permutation τ we assign the first n elements of \mathbf{Z}_τ to the set $\hat{\mathbf{X}}$ and the remaining n' to the set $\hat{\mathbf{X}}'$. Denote by $F(\cdot | \mathbf{X} \cup \mathbf{X}')$ the distribution of the scores $S = \max_{v \in V} \hat{P}E_v^\alpha(\hat{\mathbf{X}}_v \| \hat{\mathbf{X}}'_v)$ conditioned on $\mathbf{X} \cup \mathbf{X}'$, and let $\hat{q}(\mathbf{X} \cup \mathbf{X}') = \sup\{s \in \mathbb{R} \mid F(s | \mathbf{X} \cup \mathbf{X}') \leq 1 - \frac{\pi^*}{2}\}$. Then, under H_{null} , the echangeability property implies:

$$\mathbb{P}(S > \hat{q}(\mathbf{X} \cup \mathbf{X}')) = \mathbb{E}_{\mathbf{X} \cup \mathbf{X}'} \left[\mathbb{P}(S > \hat{q}(\mathbf{X} \cup \mathbf{X}') | \mathbf{X} \cup \mathbf{X}') \right] \leq \mathbb{E}_{\mathbf{X} \cup \mathbf{X}'} \left[1 - F(\hat{q}(\mathbf{X} \cup \mathbf{X}') | \mathbf{X} \cup \mathbf{X}') \right] \leq \frac{\pi^*}{2}. \quad (18)$$

In a similar manner, we can verify that for $S' = \max_{v \in V} \hat{P}E_v^\alpha(\hat{\mathbf{X}}'_v \| \hat{\mathbf{X}}_v)$:

$$\mathbb{P}(S' > \hat{q}'(\mathbf{X} \cup \mathbf{X}')) \leq \frac{\pi^*}{2}. \quad (19)$$

By putting together both inequalities, we can conclude:

$$\mathbb{P}(S > \hat{q}(\mathbf{X} \cup \mathbf{X}') \text{ or } S' > \hat{q}'(\mathbf{X} \cup \mathbf{X}')) \leq \mathbb{P}(S > \hat{q}(\mathbf{X} \cup \mathbf{X}')) + \mathbb{P}(S' > \hat{q}'(\mathbf{X} \cup \mathbf{X}')) \leq \pi^*. \quad (20)$$

And weak control over FWER comes from:

$$\begin{aligned} FWER(R_{\text{CMT}}) &= \mathbb{P}(\{\exists v : S_v > \hat{q}(\mathbf{X} \cup \mathbf{X}') \text{ or } S'_v > \hat{q}'(\mathbf{X} \cup \mathbf{X}')\} | H_{\text{null}}) \\ &\leq \mathbb{P}(\{\exists v : S_v > \hat{q}(\mathbf{X} \cup \mathbf{X}')\} | H_{\text{null}}) + \mathbb{P}(\{\exists v : S'_v > \hat{q}'(\mathbf{X} \cup \mathbf{X}')\} | H_{\text{null}}) \\ &= \mathbb{P}(S > \hat{q}(\mathbf{X} \cup \mathbf{X}') | H_{\text{null}}) + \mathbb{P}(S' > \hat{q}'(\mathbf{X} \cup \mathbf{X}') | H_{\text{null}}) \leq \pi^*. \end{aligned} \quad (21)$$

■

B. Further details about the experiments

In this section, we give more details on the implementation of the experimental setting described in the main text. Mainly:

1. More details on how the hyperparameters of GRULSIF and the other methods were chosen.
2. Elements to complement the results on the synthetic scenarios. This includes the way the AFROC and the ROC curves were estimated, and a detailed discussion about the role of the regularization parameter α used by CTST and POOL.
3. Further details on the real-world example, including the preprocessing pipeline and the figures comparing the different multiple hypothesis testing settings.

B.1. Details regarding hyperparameters selection

For RULSIF and ULSIF algorithms, we follow (Sugiyama et al., 2011a) and (Yamada et al., 2011), and the hyperapemeters are selected independently for each of the nodes. We run a leave-one-out cross-validation procedure over the parameter associated with the Gaussian kernel and the penalization term γ . The parameter σ is selected from the grid $\{0.6\sigma_{\text{median}}, 0.8\sigma_{\text{median}}, 1\sigma_{\text{median}}, 1.2\sigma_{\text{median}}, 1.4\sigma_{\text{median}}\}$ where σ_{median} is the parameter σ found via the median heuristic over the observations in X'_v . On the other hand, the penalization parameter γ is optimized from the grid $\{1e^{-5}, 1e^{-3}, 0.1, 10\}$. The procedure for KLIEP is similar, but we use instead a 5-fold cross-validation procedure.

For MMD median and MMD max, we identify the hyperparameters independently for each of the nodes, we follow the guidelines given in (Gretton et al., 2012; Sutherland et al., 2017), respectively.

Finally, for CTST and the POOL algorithms, we apply 5-fold cross-validation to select the hyperparameters σ , γ , and λ using the implementation of (de la Concha et al., 2024). Since the POOL approach ignores the graph structure, we fix $\lambda = 1$, and the penalization term related with the norm of each functional f_v will depend only on the parameter γ . In order to select the width σ for the Gaussian kernel, we first compute $\{\sigma_v\}_{v \in V}$ for each node via the median heuristic applied to the observations of X_v (such quantities are available when generating the dictionary), and we define $\sigma_{\min} = \operatorname{argmin}\{\sigma_v\}_{v \in V}$, $\sigma_{\text{median}} = \operatorname{median}\{\sigma_v\}_{v \in V}$ and $\sigma_{\max} = \operatorname{argmax}\{\sigma_v\}_{v \in V}$; we then chose the final parameter from the set $\{\sigma_{\min}, \frac{1}{2}(\sigma_{\min} + \sigma_{\text{median}}), \sigma_{\text{median}}, \frac{1}{2}(\sigma_{\max} + \sigma_{\text{median}}), \sigma_{\max}\}$. γ is selected from the set $\{1e^{-5}, 1e^{-3}, 0.1, 1\}$. Finally, we define the average node degree \bar{d} , and we identify the optimal λ^* from the set $\{1e^{-3} \cdot \frac{1}{\bar{d}}, 1e^{-2} \cdot \frac{1}{\bar{d}}, 0.1 \cdot \frac{1}{\bar{d}}, 1 \cdot \frac{1}{\bar{d}}, 10 \cdot \frac{1}{\bar{d}}\}$.

B.2. Details regarding synthetic scenarios

B.2.1. AFROC AND ROC CURVES

The *Alternative Free-response Receiver Operating Characteristic* (AFROC) curve is an important tool in the context of multiple hypothesis testing, especially in fields where the practitioner seeks a decision to a global problem while requiring correct localization for true positive events (Chakraborty & Winter, 1990). In our context, AFROC allow us to quantify to which extent the compared methods achieve *Family-wise False Positive Rate* (FWER) control under the null hypothesis that all nodes $p_v = q_v$ (see Sec. 3.3 and the H_{null} in Eq. 3), while still being sensitive enough to identify those nodes where $p_v \neq q_v$ (H_{alt}). For each of the synthetic experiments described in Tab. 3, the given input graph G according to the scenario being studied is kept fixed (see Tab. 2), and then the axis of the AFROC curves for the experiments are estimated as follows:

1. Generate 1000 synthetic experiment instances, where for all nodes $p_v = q_v$ and the graph is fixed (Null-instances).
2. Generate 1000 synthetic experiment instances that satisfy the associated schema (Tab. 2-3) (Alternative- instances).
3. For each of the Null-instances and Alternative-instances compute the node-level tests statistics associated to the MTST method used. We refer to the output of this step as processed-Null-instances and processed-Alternative-instances.
4. Threshold the processed-Null-instances and processed-Alternative-instances at the full range of possible threshold values thd (bigger than 0 value for the methods being tested), and compute the FWER and the true positive rate (TPR):
 - **FWER (x-axis)** For each threshold level, compute the fraction of processed-Null-instances where there was a least one node whose value was bigger than the fixed thd .
 - **TPR (y-axis)** For each threshold value, for each of the Alternative-instances compute the fraction of nodes where $p_v \neq q_v$ whose associated test statistic was bigger than thd . The reported TPR is the average TPR estimated over all the Alternative-instances.
5. Finally, we compute the AUC from the resulting curve limited to values of FWER in $[0.00, 0.05]$, which are the values of interest for a test of significance level 0.05.

The higher the value of the AUC of the AFROC curve, the more efficient the analyzed algorithm. We divide the result by 0.05 in order to scale the result and keep the same interpretation as for a classical AUC result.

Notice that AFROC ignores the nodes in the Alternative-instances where $p_v = q_v$ whose associated π -value is small (false rejections), thus the Null hypothesis is incorrectly rejected. To quantify how well a method differentiates the nodes that should be rejected, we estimate as well the usual ROC curves from the processed-Alternative instances and compute the associated AUC. The interpretation of the results should take AFROC-AUC as the most important criterion, and ROC-AUC rather as a tiebreaker for approaches with similar AFROC-AUC.

Finally, recall that, in a given study, the graph is not a random variable but it is rather a given fixed element, which justifies why we do not vary this element in the analysis above.

B.2.2. THE ROLE OF α

In this section, we discuss the role of parameter α in the graph-structured MTST problem. We retain the same set of experiments described in Sec. 4 to compare the role of α in CTST that integrates the graph structure, as well as in the POOL variant that does not consider the graph. The comparison relies on the AFROC-AUC and ROC-AUC measures. Results are summarized in Tab. 4.

As explained in the main text, the role of α is to upper-bound the relative likelihood-ratios r_v^α , thereby preventing convergence issues in terms of sample size and numerical instability. In previous works, such as those in (Yamada et al., 2011; de la

Table 4: Results on synthetic scenarios with variable regularization parameter α . Non-parametric methods applied on multiple two-sample testing over a known graph. Keeping the graph fixed, the AFROC and ROC curves were computed over 1000+1000 experiment instances generated over H_{null} and H_{alt} of Problem 1, respectively. Higher AUC values are better.

Experiment	Method	$n = n' = 50$		$n = n' = 100$		$n = n' = 250$	
		AFROC AUC	ROC AUC	AFROC AUC	ROC AUC	AFROC AUC	ROC AUC
Synth.Ia	CTST $\alpha=0.01$	0.57	0.90	0.76	0.96	1.00	1.00
	POOL $\alpha=0.01$	0.13	0.81	0.24	0.94	0.87	1.00
	CTST $\alpha=0.1$	0.50	0.93	0.66	0.99	0.99	1.00
	POOL $\alpha=0.1$	0.28	0.84	0.49	0.93	0.64	0.99
	CTST $\alpha=0.5$	0.57	0.92	0.72	0.97	0.98	1.00
	POOL $\alpha=0.5$	0.27	0.87	0.53	0.96	0.88	1.00
Synth.Ib	CTST $\alpha=0.01$	0.99	1.00	1.00	1.00	1.00	1.00
	POOL $\alpha=0.01$	0.53	1.00	0.91	1.00	1.00	1.00
	CTST $\alpha=0.1$	1.00	1.00	1.00	1.00	1.00	1.00
	POOL $\alpha=0.1$	0.72	1.00	0.99	1.00	1.00	1.00
	CTST $\alpha=0.5$	0.99	1.00	1.00	1.00	1.00	1.00
	POOL $\alpha=0.5$	0.41	0.99	0.85	1.00	1.00	1.00
Synth.IIa	CTST $\alpha=0.01$	0.99	1.00	1.00	1.00	1.00	1.00
	POOL $\alpha=0.01$	0.14	0.96	0.72	1.00	1.00	1.00
	CTST $\alpha=0.1$	0.94	1.00	1.00	1.00	1.00	1.00
	POOL $\alpha=0.1$	0.18	0.98	0.84	0.98	1.00	1.00
	CTST $\alpha=0.5$	0.98	1.00	1.00	1.00	1.00	1.00
	POOL $\alpha=0.5$	0.04	0.89	0.43	0.99	1.00	1.00
Synth.IIb	CTST $\alpha=0.01$	0.18	0.94	0.42	0.99	1.00	1.00
	POOL $\alpha=0.01$	0.02	0.83	0.00	0.73	0.43	0.99
	CTST $\alpha=0.1$	0.30	0.92	0.65	0.98	0.98	1.00
	POOL $\alpha=0.1$	0.02	0.84	0.12	0.95	0.78	1.00
	CTST $\alpha=0.5$	0.06	0.89	0.52	0.99	0.97	1.00
	POOL $\alpha=0.5$	0.04	0.84	0.07	0.91	0.60	0.99

Concha et al., 2023; 2024), the role of α has been made explicit as a component that controls the speed of convergence of the LRE based on the Pearson’s χ^2 -divergence. The conclusion drawn by those papers is consistent: a higher value of α will lead to a faster convergence rate. Nevertheless, a high level of α will hinder to quantify the difference between p_v and q_v via the quantity $PE^\alpha(p_v||q_v)$. In the limit case, that is $\alpha = 1$, $PE^\alpha(p_v||q_v) = 0$, meaning these measures fail to differentiate p_v and q_v regardless of the form those pdfs. Therefore, there exists a trade-off: the stability associated with high values of α versus the sensibility of $PE^\alpha(p_v||q_v)$ in distinguishing between p_v and q_v . This trade-off becomes more relevant when $PE^\alpha(p_v||q_v)$ is to be used as a test statistic to carry out hypothesis testing and detection tasks.

Findings. Tab. 4 compares CTST and POOL with $\alpha \in \{0.01, 0.1, 0.5\}$. The first notable observation is that CTST outperforms consistently POOL regardless of the value of α being used. This finding highlights the predominant role of the graph component over that of α , particularly when α is set in a range of meaningful values. The second observation is that POOL’s performance appears more sensitive to the values of α , it shows lower stability, especially when there are fewer observations. In contrast, CTST is more robust with respect to this parameter. This can be attributed to the graph-based regularization term that enforces the relative likelihood-ratios estimates to be close in the RKHS, which translates to point-wise similarity as well (see Eq. 6).

Tab. 4 does not provide a clear guideline for choosing the optimal parameter α for CM2ST. In the main text, we fix $\alpha = 0.1$ because it yielded the best results for POOL, and we generally recommend using a value of $\alpha < 0.5$ when deploying CTST.

B.2.3. FURTHER DETAILS REGARDING THE APPLICATION OF TWO-SAMPLE TESTING ON REAL SEISMIC DATA

In this section, we provide more details on the preprocessing pipeline to derive the results described in Sec. 4.2, and the additional figures showing the performance of the different methods.

Data preprocessing. As mentioned in the main text, we analyze waveforms that correspond to two seismic events that occurred in New Zealand. Seism A is of magnitude 5.5, while Seism B is magnitude 2.6. These seismic events are part of the publicly available dataset provided by GeoNet. We used the Python package ObsPy to access the data (Beyreuther et al., 2010).

To study the evolution of seismic activity associated to these events, we retrieve the waveforms from 50 seconds before to 50

seconds after the event. These waveforms correspond to the measurements provided by strong-motion accelerometers that monitor shaking in three perpendicular directions. Therefore, here the input space is $\mathcal{X} \subseteq \mathbb{R}^3$. In each of the scenarios, we limit our attention to stations that had recorded observations for all the three directions during all the analyzed time period.

There are three main characteristic that are required to implement CTST in practice:

1. The relative likelihood-ratios $\{r_v^\alpha\}_{v \in V}$ are expected to be approximated by the same RKHS.
2. The FWER control of CTST (see Theorem 3.1) requires that the observations $\mathbf{X} = \{X_v\}_{v \in V} = \{x_{v,1}, \dots, x_{v,n}\}_{v \in V}$ are iid for each node v , and the same for and $\mathbf{X}' = \{X'_v\}_{v \in V} = \{x'_{v,1}, \dots, x'_{v,n'}\}_{v \in V}$.
3. The vector-valued function $\mathbf{r}^\alpha = (r_1, \dots, r_N)$ is expected to be smooth with respect to the graph G , i.e. $\|r_u - r_v\|_{\mathbb{H}} < \epsilon$ for connected nodes.

The preprocessing aims to transform and prepare the data so they satisfy these conditions.

We follow the preprocessing pipeline described in (Chen et al., 2021) with the toolbox for Seismology ObsPy. The preprocessing is performed independently for each station and independently for each direction. We start by steps that are considered to be standard in seismology: we remove the linear trend and we apply a 2-16 bandpass filter. To reduce the temporal dependency, we compute a root mean square amplitude envelope, then we fit an autoregressive model of order 1, and we keep the residuals from this model. The output is standardized so that it has zero mean and unit variance. To make the data comparable between stations, we divide the output by its maximum value.

Our objective is to provide a visualization that captures the evolution of the seismic event using the measurements available at each station. To this end, we use a graph-structured MTST to identify the specific moments and locations (stations) where the seismic activity appeared to be statistically significant. In this context, $v \in V$ denotes that station v belongs to the set of stations V . To define the statistical test, we need to identify the samples \mathbf{X} and \mathbf{X}' (see Eq. 3) that should be compared across the spatial and temporal dimensions. We denote by τ the time-stamp of the seismic event, then we consider the preprocessed observations in two time frames: $[\tau - 50, \dots, \tau)$ and $[\tau, \dots, \tau + 50)$, i.e. from 50 seconds before τ to 50 seconds after τ . These periods are segmented into 10 time-windows ($\mathcal{T} = \{1, \dots, 10\}$, each of 5 seconds duration) made of 100 preprocessed observations in each of them. According to our notation, $X_{v,1}$ is the first 100 observations at station v after $\tau - 50$, while $X'_{v,1}$ denotes the first 100 observations post-event (τ). Following the same logic, $X_{v,2}$ has the observations after $\tau - 45$ at station v , while $X'_{v,1}$ denotes the first 100 observations after $\tau + 5$. This segmentation yields two samples for each location-time pair $(v, t) \in V \times \mathcal{T}$, $X_{(v,t)} = \{x_{((v,t),i)}\}_{i=1}^{100} \sim p_{(v,t)}$ and $X'_{(v,t)} = \{x'_{((v,t),i)}\}_{i=1}^{100} \sim q_{(v,t)}$. Then, the MTST compares the pdfs $\{p_{(v,t)}\}_{(v,t) \in V \times \mathcal{T}}$ and $\{q_{(v,t)}\}_{(v,t) \in V \times \mathcal{T}}$. Alternatives can be implemented for defining different observations to consider from $\{p_{(v,t)}\}_{(v,t) \in V \times \mathcal{T}}$ to be used to compare with the post-event alternative.

The sets $\mathbf{X} = \{X_{(v,t)}\}_{v \in V, t \in \mathcal{T}}$ and $\mathbf{X}' = \{X'_{(v,t)}\}_{v \in V, t \in \mathcal{T}}$ represent the observations available at the graph G_{SXT} whose nodes represent a position in space and in time. As in the general graph-structure hypothesis testing problem, G_{SXT} encodes the expected similarity between the results of the test. To encode the fact that close stations are expected to affect each other (recall the *first law of Geography* from Sec. 1), we generate an unweighted spatial graph $G_S = (V, E, W)$ where the nodes represent the geographical positions of the seismic stations and the edges are computed in order to form a 3-nearest neighbors graph. To account for the temporal component similarity expected from the propagation of the seismic waves through the earth, we build an unweighted multiplex network $G_{\text{SXT}} = (V_T, E_T, W_T)$ on top of G_S . The set of nodes is then the pair $(v, t) \in V_T := V \times \mathcal{T}$, where V denotes the set of nodes of G_S . Two nodes in G_{SXT} , (u, t) and (v, t') , are connected: i) if $t = t'$ and $(u, v) \in E$, i.e. they refer to the same time-window and the nodes u and v are connected in the spatial graph G_S , ii) or if $u = v$ and $|t' - t| = 1$, i.e. each node $v \in V$ is connected to its ‘copies’ in the two adjacent time-windows.

The implementation details of the statistical methods being compared are the same as in the synthetic scenarios, which include the hyperparameters selection related to the estimation of the non-parametric test statistics and the way the permutation test is run.

Findings. Fig. 3-6 and Fig. 7-11 illustrate the output of the graph-structured MTST applied to the waveforms related to each for the two seismic events, Seism A and Seism B. The figures highlight the biggest connected component C_{SXT} made of pairs $(v, t) \in V_T$ that were identified as statistically significant by the method being used. In this application, we called a pair to be statistically significant if its π -value is smaller than 0.05.

We try to show in the figures both dimensions of the test. The graph on the left highlights in red the stations $v \in V$ which were elements of the biggest connected component C_T for at least one time-window, That is, there exist $t \in \mathcal{T} = \{1, \dots, 10\}$ such that $(v, t) \in C_T$. The epicenter is marked by a red star. The time-series at the left show both preprocessed data samples

$X_{(v,t)} = \{x_{((v,t),i)}\}_{i=1}^{100} \sim p_{(v,t)}$ (green time-series) and $X'_{(v,t)} = \{x'_{((v,t),i)}\}_{i=1}^{100} \sim q_{(v,t)}$ (red time-series) for the highlighted stations. The periods that were considered statistically significant are delineated by blue/pink colors (we use two colors to differentiate adjacent time-windows where the test rejected the $H_{\text{null},v}$ hypothesis).

The first thing to notice is that all methods identified the stations that were closer to the epicenter as locations where there was statistically significant evidence of a change. Algorithms that neglect the graph component tend to identify a larger number of time-windows. Upon closer inspection, we can see that many of the identified time-windows appear to be false positives, lacking in global relevance or consistency with the expected evolution of the seismic activity. Intuitively, for a short time-period around an event (here we analyze 100 seconds overall), we expect the event to alter the behavior of the measurements during consecutive time-windows, and this effect will vanish with time. This pattern is not evident in methods that disregard the spatial and temporal similarity. In contrast, CTST identifies correctly nodes close to the epicenter, and captures the evolution of the seismic activity in a more consistent way. The results are consistent with those obtained from synthetic experiments, where CTST demonstrated superior performance in terms of the AFROC-AUC. This performance also indicates the effective weak FWER control and higher sensitivity in pinpointing the nodes where $p_v \neq q_v$.

From the practitioners' perspective, MT is usually an initial exploratory tool, where tests identified as statistically significant are further inspected with further analysis. In this sense, false positives may translate to a high cost, since they may lead to the allocation of resources towards the wrong direction. Thus, the accuracy of identifying nodes where $p_v \neq q_v$ is not just a statistical concern, but also a practical one, directly impacting the efficiency and effectiveness of subsequent research efforts.

Figure 3: Seism A in New Zealand (1 of 4).

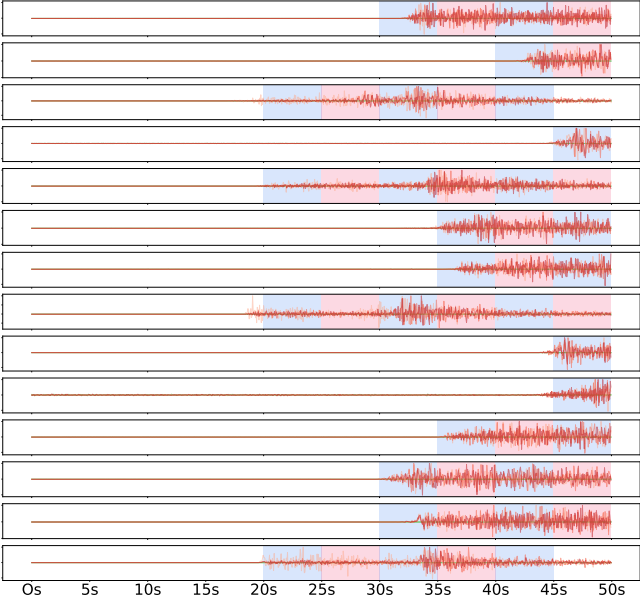
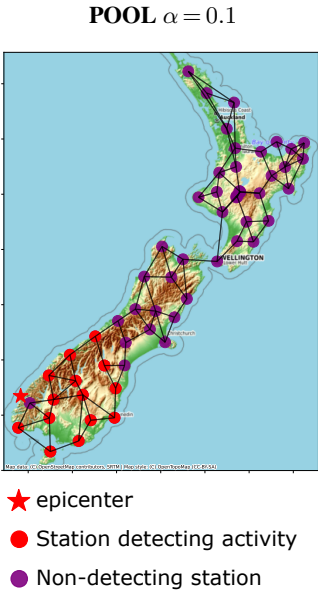
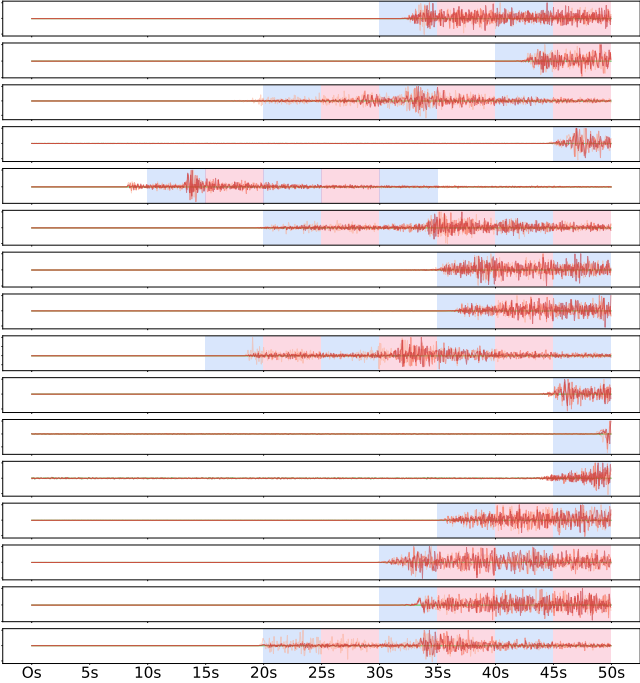
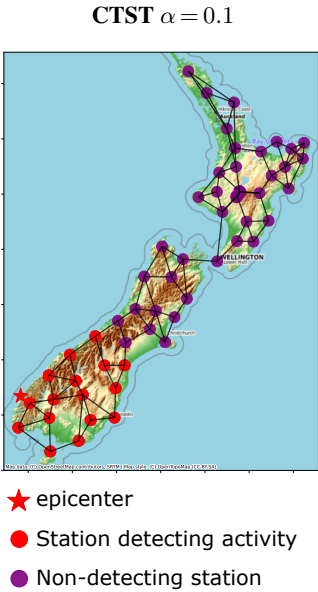


Figure 4: Seism A in New Zealand (2 of 4).

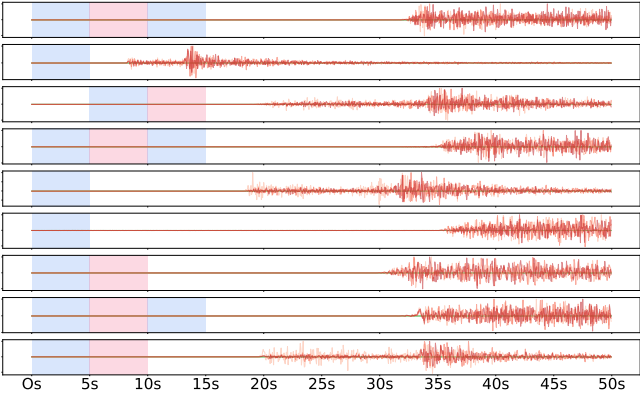
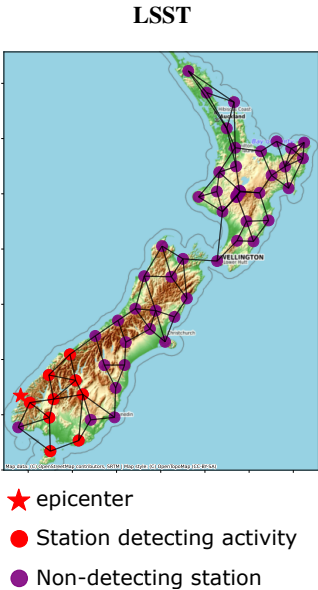
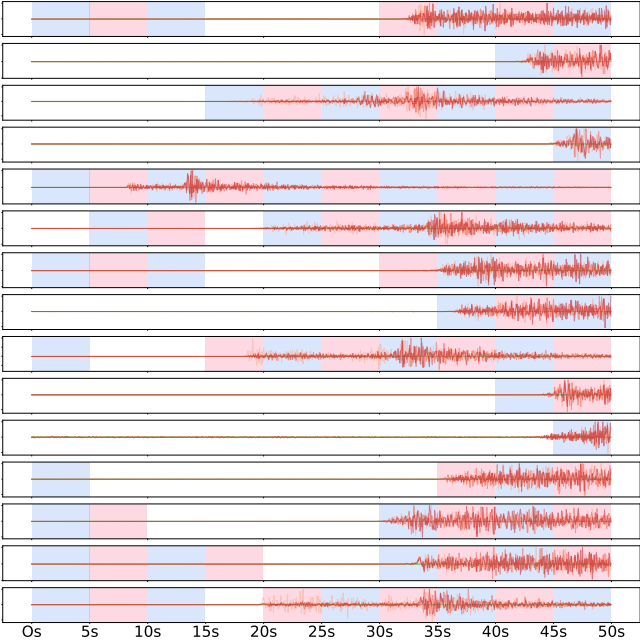
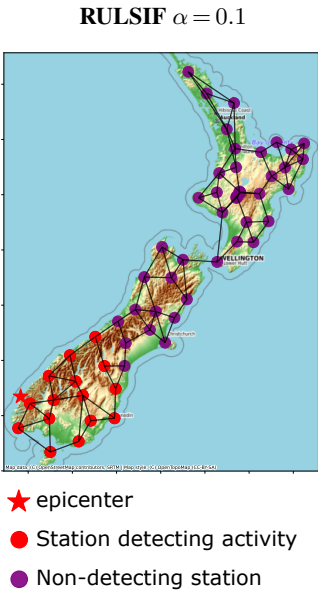


Figure 5: Seism A in New Zealand (3 of 4).

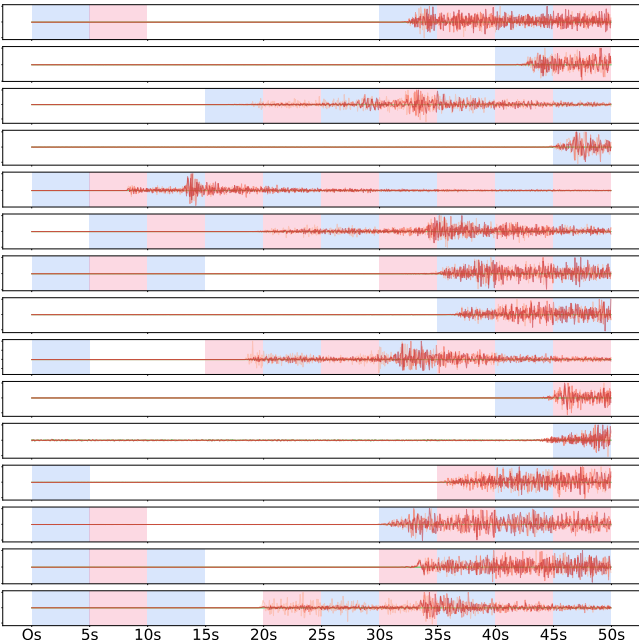
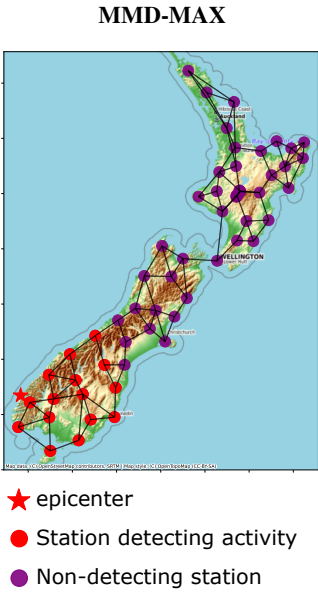
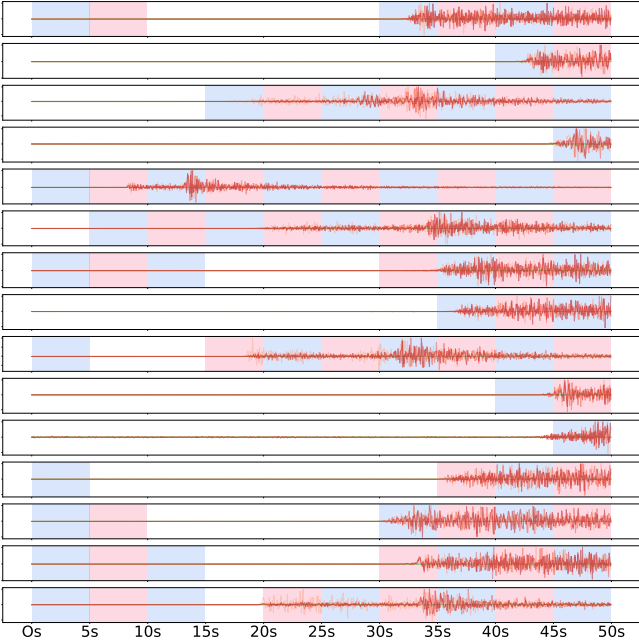
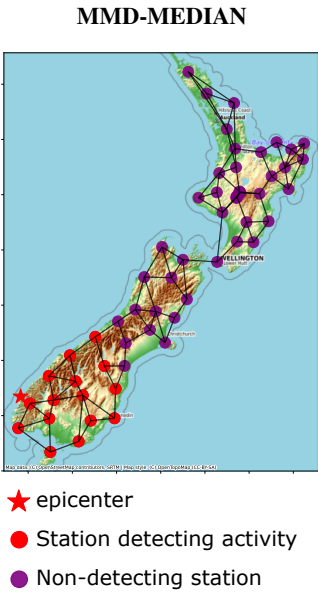


Figure 6: Seism A in New Zealand (4 of 4).

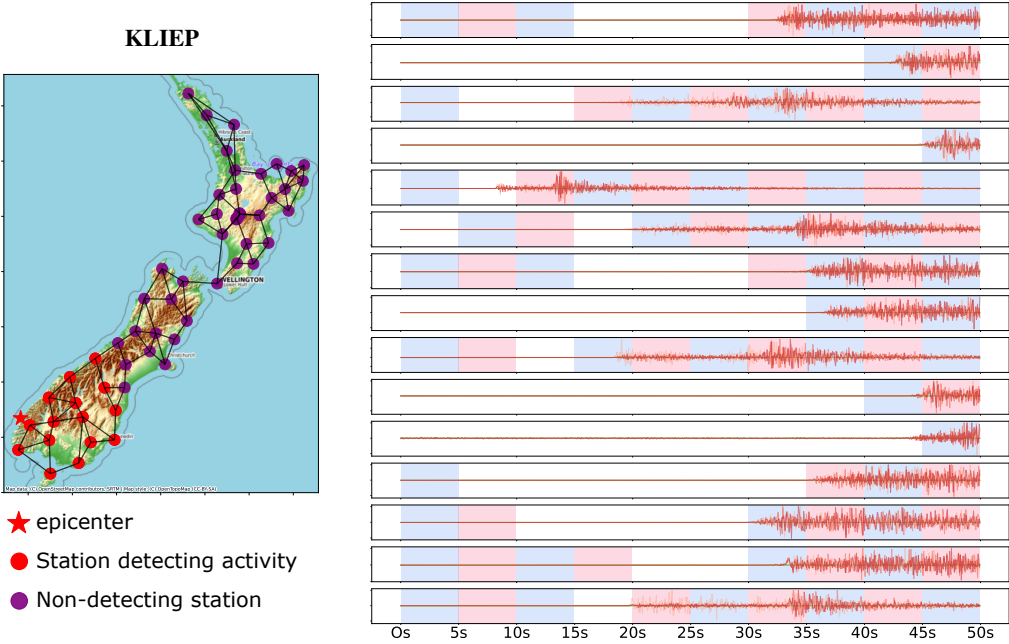


Figure 7: Seism B in New Zealand (1 of 5).

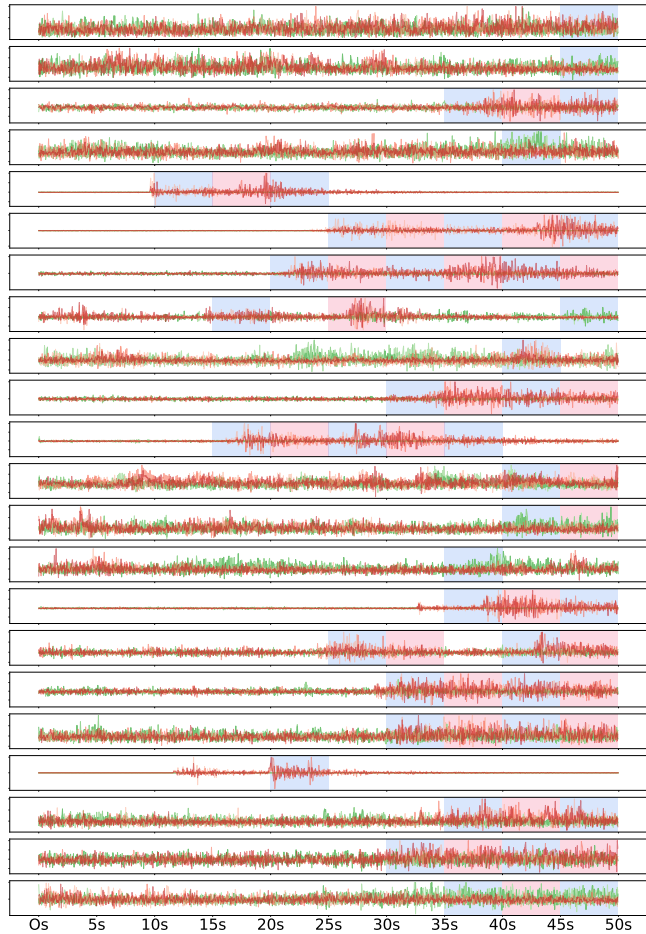
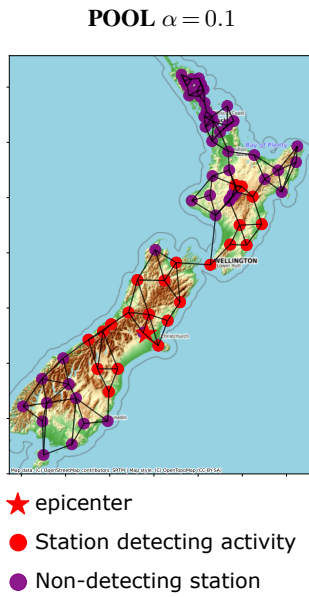
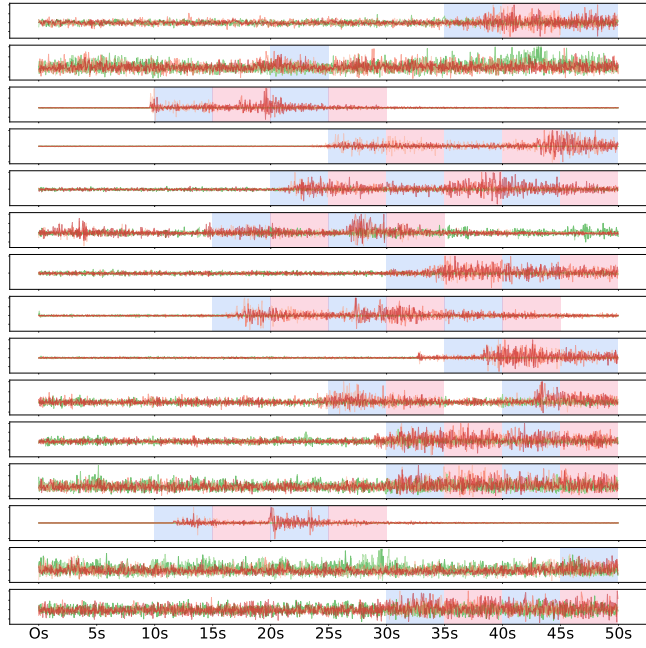
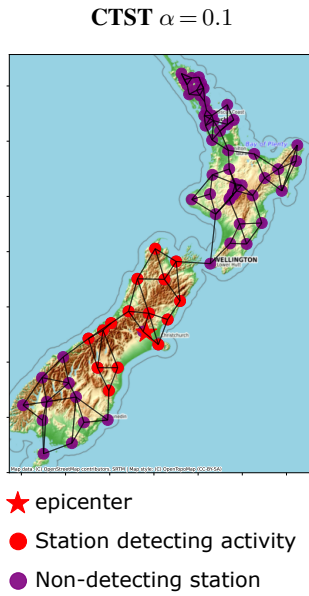


Figure 8: Seism B in New Zealand (2 of 5).

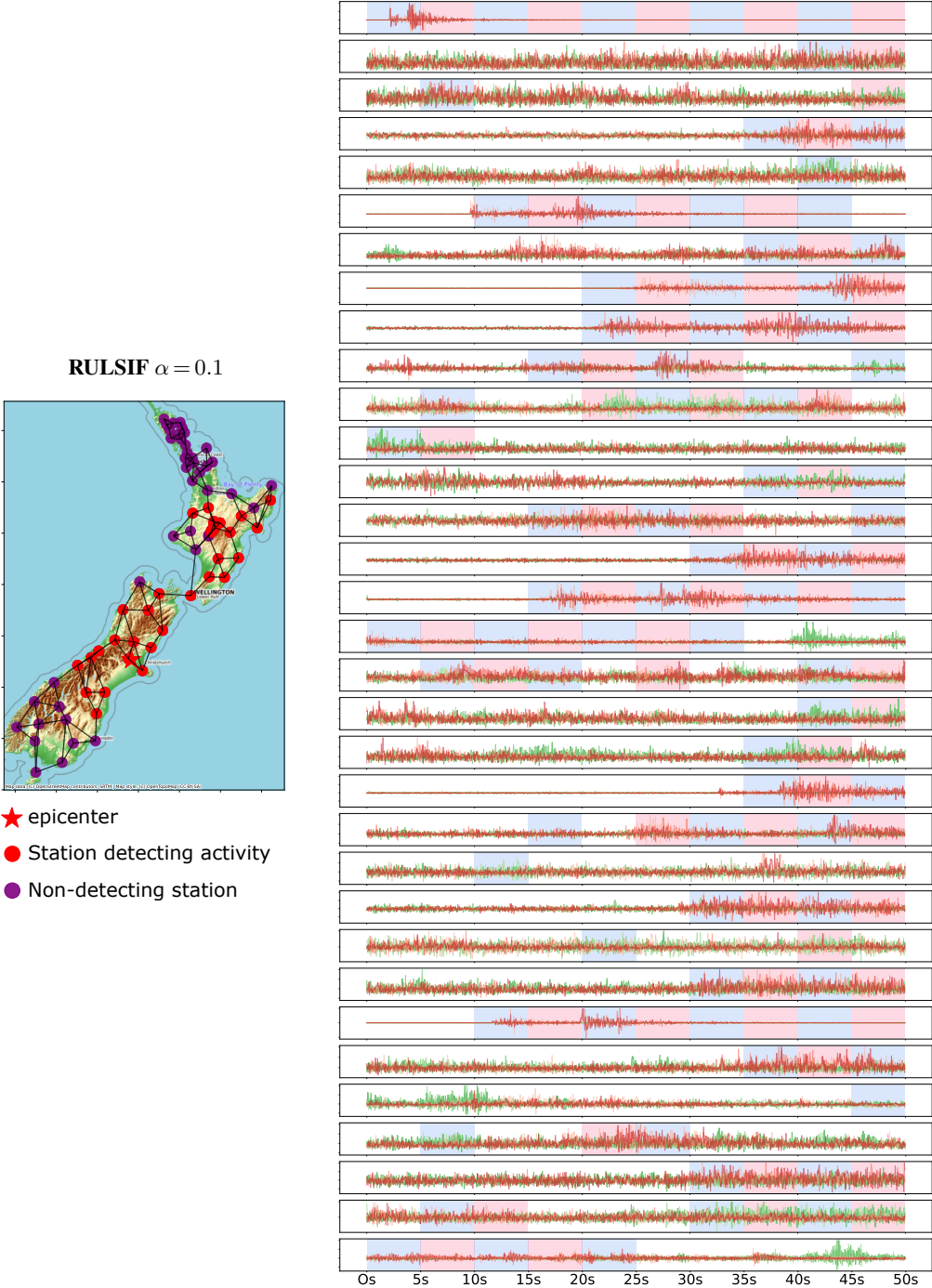


Figure 9: Seism B in New Zealand (3 of 5).

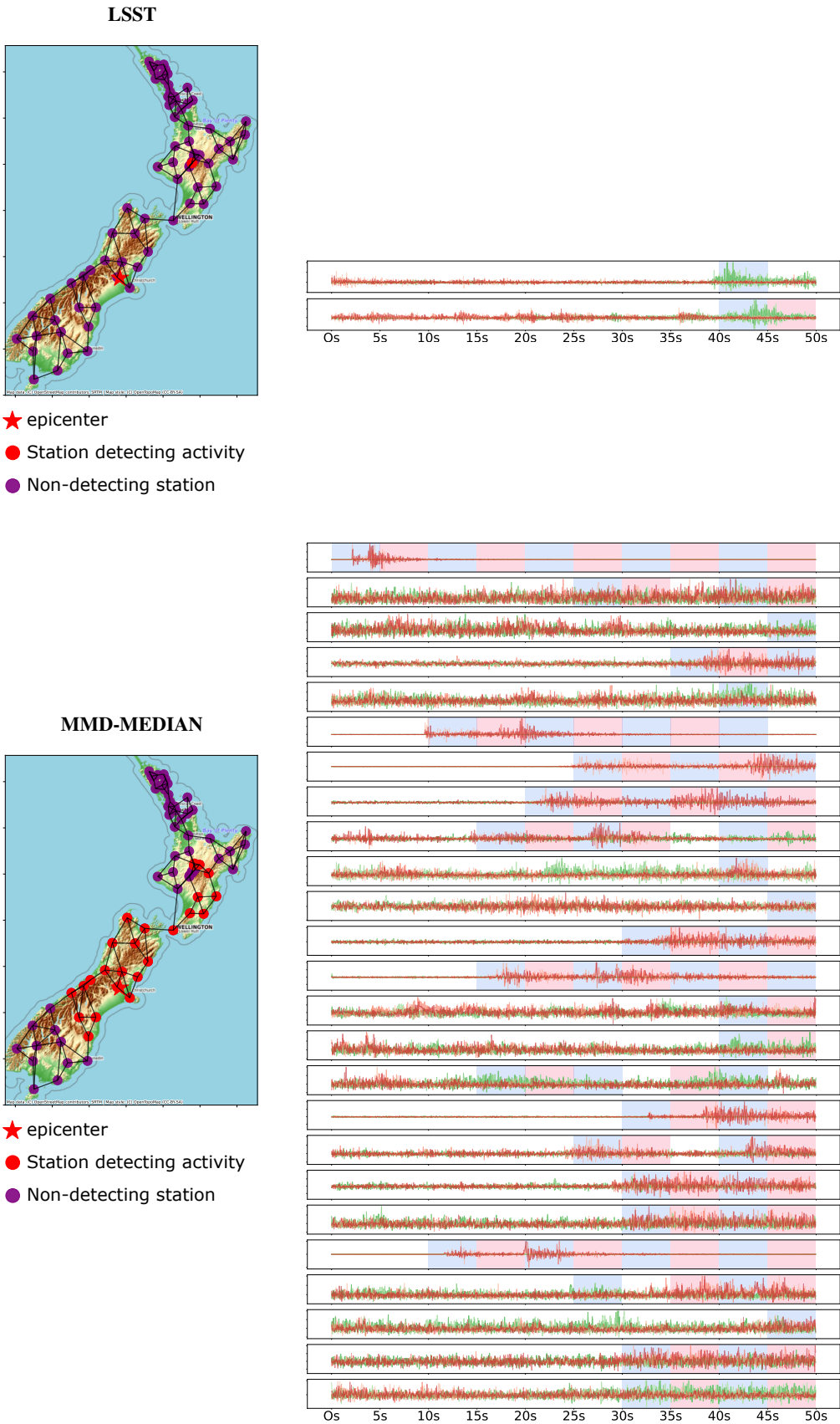


Figure 10: Seism B in New Zealand (4 of 5).

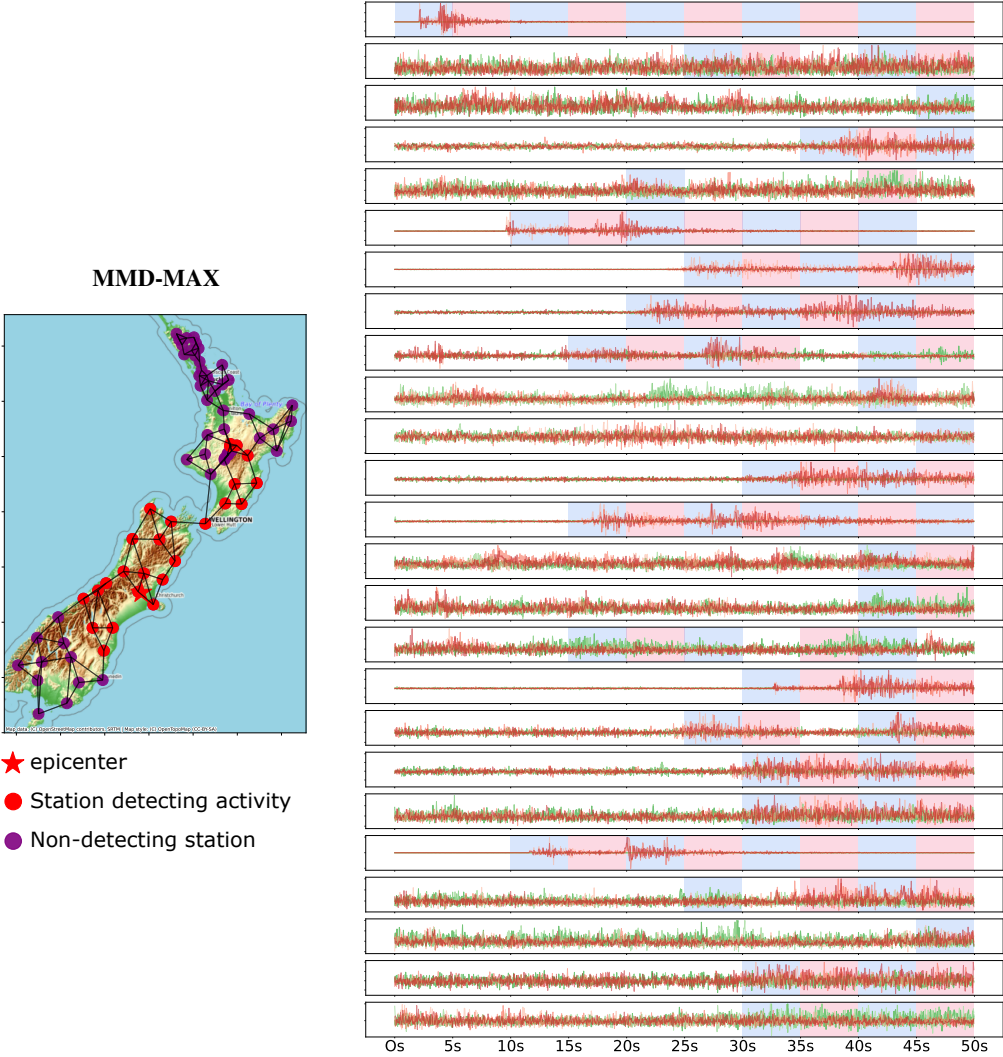


Figure 11: Seism B in New Zealand (5 of 5).

